

University of Wollongong

Research Online

Faculty of Science, Medicine and Health -
Papers: part A

Faculty of Science, Medicine and Health

1-1-2017

New ages for the Upper Palaeolithic site of Xibaimaying in the Nihewan Basin, northern China: implications for small-tool and microblade industries in north-east Asia during Marine Isotope Stages 2 and 3

Yujie Guo

Peking University, yg991@uowmail.edu.au

Bo Li

University of Wollongong, bli@uow.edu.au

Jia-Fu Zhang

Peking University

Bao Yin Yuan

Chinese Academy Of Sciences

Fei Xie

Cultural Relics Of Hebei Province

Follow this and additional works at: <https://ro.uow.edu.au/smhpapers>



Part of the [Medicine and Health Sciences Commons](#), and the [Social and Behavioral Sciences Commons](#)
See next page for additional authors

Recommended Citation

Guo, Yujie; Li, Bo; Zhang, Jia-Fu; Yuan, Bao Yin; Xie, Fei; and Roberts, Richard G., "New ages for the Upper Palaeolithic site of Xibaimaying in the Nihewan Basin, northern China: implications for small-tool and microblade industries in north-east Asia during Marine Isotope Stages 2 and 3" (2017). *Faculty of Science, Medicine and Health - Papers: part A*. 4678.
<https://ro.uow.edu.au/smhpapers/4678>

Research Online is the open access institutional repository for the University of Wollongong. For further information contact the UOW Library: research-pubs@uow.edu.au

New ages for the Upper Palaeolithic site of Xibaimaying in the Nihewan Basin, northern China: implications for small-tool and microblade industries in north-east Asia during Marine Isotope Stages 2 and 3

Abstract

It has been suggested that the 'small-tool' and microblade Upper Palaeolithic industries coexisted in the Nihewan Basin of northern China for about 8-14 000 years during Marine Isotope Stage (MIS) 2. This inference was based on uranium-series ages of around 15 and 18 ka for bovid teeth recovered from the 'latest' small-tool site of Xibaimaying - the youngest occurrence of such tools in the region - and optically stimulated luminescence (OSL) dating of the earliest typical microblade site (Youfang: ~26-29 ka). In this study, we re-dated the Xibaimaying site using single-grain OSL methods and the resulting ages indicate that the cultural layer was deposited 46 ± 3 ka ago, during MIS 3 - more than 20 millennia earlier than previously thought and older also than the so-called earliest 'primitive' and typical microblade tools found at Zhiyu (~31-39 ka cal BP) and Youfang. These new ages for human occupation of Xibaimaying remove support for the parallel development of the small-tool and microblade industries in the Nihewan Basin during the Upper Palaeolithic, but reliable age estimates from additional sites are needed to confidently infer the nature of the chronological relationship between these two Upper Palaeolithic industries and the associated toolmakers.

Disciplines

Medicine and Health Sciences | Social and Behavioral Sciences

Publication Details

Guo, Y., Li, B., Zhang, J., Yuan, B., Xie, F. & Roberts, R. G. (2017). New ages for the Upper Palaeolithic site of Xibaimaying in the Nihewan Basin, northern China: implications for small-tool and microblade industries in north-east Asia during Marine Isotope Stages 2 and 3. *Journal of Quaternary Science*, 32 (4), 540-552.

Authors

Yujie Guo, Bo Li, Jia-Fu Zhang, Bao Yin Yuan, Fei Xie, and Richard G. Roberts

1 New ages for the Upper Palaeolithic site of
2 Xibaimaying in the Nihewan Basin, northern
3 China: implications for small-tool and microblade
4 industries in northeast Asia during Marine Isotope
5 Stages 2 and 3

6 Yu-Jie Guo^{1*}, Bo Li¹, Jia-Fu Zhang², Bao-Yin Yuan³, Fei Xie⁴, Richard G. Roberts¹

7 ¹ *Centre for Archaeological Science, School of Earth and Environmental Sciences, University of*
8 *Wollongong, Wollongong, NSW 2522, Australia*

9 ² *MOE Laboratory for Earth Surface Processes, Department of Geography, College of Urban and*
10 *Environmental Sciences, Peking University, Beijing 100871, China*

11 ³ *Institute of Geology and Geophysics, Chinese Academy of Sciences, Beijing 100029, China*

12 ⁴ *Cultural Relics of Hebei Province, Shijiazhuang 050000, China*

13 * Corresponding author: yj991@uowmail.edu.au; yjguo87@gmail.com

14

15

16

17

18

19

20 Abstract

21 It has been suggested that the 'small tool' and microblade Upper Palaeolithic
22 industries coexisted in the Nihewan Basin of northern China for about 8–14 thousand
23 years during Marine Isotope Stage (MIS) 2. This inference was based on uranium-
24 series ages of around 15 and 18 ka for bovid teeth recovered from the 'latest' small-
25 tool site of Xibaimaying—the youngest occurrence of such tools in the region—and
26 optically stimulated luminescence (OSL) dating of the earliest typical microblade site
27 (Youfang: ~26–29 ka). In this study, we re-dated the Xibaimaying site using single-
28 grain OSL methods and the resulting ages indicate that the cultural layer was
29 deposited 46 ± 3 ka ago, during MIS 3—more than 20 millennia earlier than
30 previously thought and older also than the so-called earliest 'primitive' and typical
31 microblade tools found at Zhiyu (~31–39 ka cal BP) and Youfang. These new ages
32 for human occupation of Xibaimaying remove support for the parallel development of
33 the small-tool and microblade industries in the Nihewan Basin during the Upper
34 Palaeolithic, but reliable age estimates from additional sites are needed to
35 confidently infer the nature of the chronological relationship between these two
36 Upper Palaeolithic industries and the associated toolmakers.

37 **Keywords:** quartz OSL; single-grain dating; Chinese Palaeolithic; stone artefacts;
38 MIS 3.

39

40 Introduction

41 The 'small tool' industry is one of the two major Palaeolithic traditions in North
42 China (Jia et al., 1972). It was first recognised and classified as the Zhoukoudian
43 Locality 1–Zhiyu series (in the boat-shaped scrapers–burins tradition) (Jia et al.,
44 1972), and was later named the small-tool technology or industry (Zhang, 1990; Liu,
45 2014). The small-tool assemblage is characterised by rare prepared cores and
46 production of small, irregular flakes, some of which were probably used as scrapers
47 (Zhang, 1999). The small-tool industry is considered to be the most abundant
48 Palaeolithic industry known from northern China during the Pleistocene (Zhang,
49 1999), found across northern China ($107^{\circ}29'$ – $122^{\circ}10'$ E, $34^{\circ}10'$ – $41^{\circ}15'$ N) during the
50 Lower and Middle Palaeolithic and across almost all of China ($87^{\circ}21'$ – $126^{\circ}18'$ E,
51 $24^{\circ}55'$ – $45^{\circ}36'$ N) in the Upper Palaeolithic (Fig. 1) (Zhang, 1999). Representative
52 sites include Zhoukoudian Locality 1 (Teihard de Chardin and Pei, 1932),
53 Zhoukoudian Locality 15 (Gai, 1991), Salawusu (Teihard de Chardin and Licent,
54 1924), Zhiyu (Jia et al., 1972) and Xiaonanhai (An, 1965) (Fig. 1).

55 The small-tool industry is commonly considered to have originated and
56 developed primarily in the Nihewan Basin (Fig. 1) since the Early Pleistocene (Liu,
57 2014). The Basin is key to the study of the Palaeolithic archaeology of East Asia,
58 with more than 100 Palaeolithic sites spanning the entire Pleistocene (e.g., Schick et
59 al., 1991; Zhu et al., 2001, 2004; Hou, 2008; Norton and Gao, 2008; Nian et al.,
60 2014; Guo et al., 2016). The small-tool industry is considered to be 'continuous' from
61 the Early to the Late Pleistocene (Liu et al., 2013), whereas the typical microblade
62 industry emerged ~29 ka ago in this region (Nian et al., 2014). Representative small-
63 tool sites in the Basin include Heitugou (~1.77–1.95 Ma: Wei et al., 2016),
64 Majuangou (~1.66 Ma: Zhu et al., 2004), Xiaochangliang (~1.36 Ma: Zhu et al.,

65 2001), Donggutuo (~1.1 Ma: Wang et al., 2005), Sankeshu (~200–300 ka: Hou et al.,
66 2010), Xujiayao (~240 ka: Tu et al., 2015, or ~220–160 ka: Mu et al., 2015 and
67 Zhang et al., 2015), Banjingzi (~86 ka: Guo et al., 2016), Zhiyu (~31–36 ka cal BP:
68 Institute of Archaeology of Chinese Academy of Social Sciences, 1991, or ~36–39 ka
69 cal BP: Yuan, 1993; and discussed further below) and Xibaimaying (~15–18 ka: Xie
70 and Yu, 1989). These form an ‘evolutionary line’ for the small-tool industry during the
71 Pleistocene (Liu, 2014).

72 Although the small-tool industry appears to have developed gradually in the
73 Nihewan Basin over the last two million years, some ‘advanced’ or ‘developed’ traits
74 have been reported at several sites, including Donggutuo, Xujiayao, Banjingzi and
75 Zhiyu (Liu et al., 2013; Liu, 2014). One of the most important discoveries associated
76 with small-tool lithic assemblages is the prepared, wedge-shaped core found at
77 Donggutuo (the so-called ‘Donggutuo Core’: Hou et al., 1999; Hou, 2003, 2008).
78 Some archaeologists consider the ‘Donggutuo Core’, which was used to produce
79 small elongated flakes, as the ancestral form of the wedge-shaped, microblade cores
80 found at Upper Palaeolithic sites across northeast Asia (Hou et al., 1999; Hou, 2003,
81 2008). Donggutuo Cores (or their equivalent) have also been described from the
82 sites of Sankeshu, Xujiayao and Zhiyu in the Nihewan Basin, Zhoukoudian Localities
83 1 and 15 and Shuidonggou in northern China (Liu et al., 2013), Kara-Bom, Denisova
84 and Ust-Karakol in southern Siberia (Hou, 2005), and Chikhen Agui Cave in
85 Mongolia (Derevianko, 2001).

86 During the Upper Palaeolithic, lithic technologies in the Nihewan Basin became
87 more complex. It has been argued that the microblade culture and the small tool
88 culture “developed simultaneously, but without mutual influence” (Liu et al., 2013).
89 Animal bone fragments from the Zhiyu site have been dated by ¹⁴C to 28,945 ± 1370

90 BP (Institute of Archaeology of Chinese Academy of Social Sciences, 1991) and
91 $33,155 \pm 645$ BP (Yuan, 1993), which correspond to calendar-year ages (95%
92 confidence intervals) of 30.5–35.7 and 35.8–38.8 ka cal BP, respectively. The lithic
93 technology at this site has been described as ‘transitional’ between small-tool and
94 microblade (Jia et al., 1972; Jia, 1978) or ‘primitive’ microblade (Chun, 1984).
95 According to some other archaeologists, the stone artefacts at this site may not be
96 related to microblade technology, but their alternative interpretations have yet to be
97 published. The Youfang site—dated to about 26–29 ka based on OSL analyses of
98 quartz grains (Nian et al., 2014)—is considered to be the earliest ‘typical’ microblade
99 site known from the northern high latitudes of China (40°N) (Nian et al., 2014), while
100 the Xibaimaying site is considered to be the ‘latest’ small-tool site discovered in the
101 Nihewan Basin (Xie et al., 2006). The age range of ~15–18 ka for Xibaimaying is
102 based on uranium-series dating of bovid teeth (Xie and Yu, 1989). These ages,
103 together with those for Zhiyu and Youfang, have led to the suggestion that the small-
104 tool and microblade industries coexisted in the Nihewan Basin (Xie et al., 2006; Liu
105 et al., 2013; Jia et al., 2015) from at least ~30 ka ago until as recently as ~15 ka ago.

106 The coexistence of these two industries raises a number of questions, including
107 the reason for the lack of technological ‘development’ at Xibaimaying, the youngest
108 of these sites. Jia et al. (2015) showed that the availability of raw material was not
109 the main factor governing the absence of microblade technology at this site. They
110 also argued that microblade technology did not appear to spread as an adaptive
111 response to deteriorating environmental conditions associated with the Last Glacial
112 Maximum (LGM), ~21 ka ago, as has been hypothesised previously (Institute of
113 Archaeology of Northern Ethnicity and Department of Archaeology and Museology,
114 Renmin University, 2006). Others have proposed that microblade technology was

115 introduced to northern China by people migrating from Siberia or Mongolia (e.g.,
116 Keates, 2007; Kuzmin, 2007; Nian et al., 2014), whereas Xibaimaying might be
117 inhabited by a local group who maintained their small-tool tradition (Jia et al., 2015).
118 If so, then the prehistory of the Nihewan Basin might be much complex than
119 currently thought (Liu et al., 2013).

120 These archaeological discussions are based on the presumption that the ages
121 for Xibaimaying and Youfang are accurate, which may not be true. In particular,
122 uranium-series dating is now well-known to be poorly suited to faunal remains, owing
123 to their open-system geochemical behaviour (Hellstrom and Pickering, 2015).
124 Uranium-series dating typically provides only minimum age estimates for fossil
125 bones and teeth, even when modern methods of data collection and analysis are
126 used (Grün et al., 2014). In view of the questionable accuracy of the uranium-series
127 ages for Xibaimaying, the aim of this study is to provide more reliable estimates of
128 age for human occupation of this 'latest' small-tool site using OSL dating methods
129 applied to quartz grains. This method has previously been applied to deposits
130 elsewhere in the Nihewan Basin (e.g., Zhao et al., 2010; Nian et al., 2014; Guo et al.,
131 2015, 2016), so OSL dating of Xibaimaying would enable a direct chronological
132 comparison with other sites in the region—including the microblade site of Youfang.

133 The study site

134 The Xibaimaying site (40°07'28"N, 114°14'19"E, 915 m above mean sea level)
135 is located on the second terrace of the east bank of the Nangou gully (Fig. 2a), a
136 tributary of the Sanggan River, ~300 m south of Xibaimaying village in Yangyuan
137 County of Hebei Province (Xie et al., 2006). The site was discovered in 1985 and a
138 total area of 76 m² excavated in 1985 and 1986. The sedimentary profile of the east

139 wall of the excavation pit consists of 5 layers (Fig. 2b,d), which are as follows (top to
140 bottom): soil (~0.1 m in depth), red-yellow silty clay (~0.7 m), white-yellow silty clay
141 (~0.5 m), yellow silty clay (~1.4 m) and fluvially interbedded grey-green and red-
142 yellow clayey fine sands (~0.4 m). The basal unit (Layer 5) yielded abundant stone
143 artefacts, animal bone remains (Fig. 2c), burnt soil blocks, burnt bones and charcoal,
144 and represents the cultural layer at this site (Xie and Yu, 1989).

145 A total of 1546 stone artefacts have been recovered from the cultural layer at
146 this site (Xie and Yu, 1989), including cores (n = 78), flakes (n = 184), tools (n = 230)
147 and waste objects (e.g., chunks, debris; n = 1054) produced during the process of
148 lithic reduction. Some typical stone artefacts are shown in Fig. 3. The general
149 properties of the stone artefacts are described by Xie and Yu (1989) in Chinese, so
150 we have summarised them below in English:

151 (1) Cores include 75 hammered cores and 3 percussion cores. Most of the
152 hammered cores are small, with the largest and smallest being 104×74×52 mm
153 and 18×10×9 mm in size, respectively. The hammered cores can be further
154 divided into single platform (n = 31), double platform (n = 27) and multi-platform
155 (n = 17). Platforms are dominated by plain platforms, followed by natural
156 platforms; scarred platforms are rare. Some multi-platform cores are nearly
157 spheroidal in shape. Several single-platform cores (Fig. 3i,j) show some traits of
158 micro-cores: cone-shaped with plain platforms and flaking scars that are
159 elongated and dense. The three percussion cores are small in size (< 30 mm)
160 and slightly elongated in shape (Fig. 3k,l).

161 (2) Flakes are composed of hammered flakes (n = 179) and percussion flakes (n =
162 5). The flake platforms are dominated by plain platforms, followed by natural

163 platforms and scarred platforms; prepared platforms are rare. Flakes are
164 generally irregular in shape, but dominated by flakes that are wider than they are
165 long. Most of the flakes are small in size, with the largest and smallest being
166 92×98×25 mm and 8×12×3 mm, respectively.

167 (3) Tools are commonly less than 40 mm in maximum dimension, dominated by
168 scrapers (n = 216) associated with points (n = 11), burins (n = 2) and a chopper
169 (n = 1). The tool blanks are mainly flakes (66%) and chunks (34%). The fracture
170 method was mainly hammering. Most of the tools are retouched, with fine regular
171 scars, and several scrapers have been retouched by indirect pressure.

172 (4) Raw materials are dominated by pyroclastic rock (35.6%) associated with vein
173 quartz (18.6%), agate (13.6%), siliceous limestone (12.7%), flint (9.9%),
174 hornstone (6.1%), quartz sandstone (2.1%) and schist (1.4%). The tools,
175 however, are mostly made from flint and agate. Du (2003) analysed the raw
176 materials at Xibaimaying and argued that the agate, flint and vein quartz are
177 similar as those at the Shenquansi site (Fig. 1), the pyroclastic rocks are similar
178 to those at the Xinmiaozihuang site (Fig. 1) and the occupants of Xibaimaying
179 had no preference for a particular raw material type; all the raw materials are
180 available within ~10 km of the site (Du, 2003).

181 The cultural layer contains abundant vertebrate and freshwater mollusc fossils
182 (Xie and Yu, 1989). The identified freshwater molluscs include *Corbicula fluminea*,
183 *Gyraulus convediusculus*, *G. compressus* and *Radxi auricularia*. The identified
184 vertebrate fossils include *Strothio* sp. (ostrich), *Bos primigenius* (cow), *Equus*
185 *pnzewalskyi* (horse), *E. hemionus* (donkey), *Gazella przewalskyi* (antelope), *Cervus*
186 sp. (deer), *Sus* sp. (pig), *Coelodonta* sp. (rhinoceros), *Elephas* sp (elephant) and

187 Carnivora (not identifiable to genus or species). A total of 315 fossil bones, most of
188 which are broken, were analysed by Xie and Yu (1989); 24 bones had been gnawed
189 by rodents and 31 were identified as bone tools (e.g., Fig. 3m). The artefacts from
190 this site are thought to be in primary depositional context, based on the well-
191 preserved state of the cultural remains and the lack of evidence of any disturbance
192 of the artefact-bearing layer (Xie et al., 2006). This site was probably used to
193 manufacture stone tools, with the lithic reduction process accounting for the large
194 number of waste objects recovered (Xie et al., 2006). Two uranium-series ages of 18
195 ± 1 and 15 ± 1 ka were obtained for bovid teeth from the cultural layer (Xie and Yu,
196 1989), on which basis the site was assigned to the Upper Palaeolithic.

197 In this study, five sediment samples (XBMY-OSL-1 to -5) were collected from
198 the sedimentary profile at Xibaimaying (Fig. 2). Only four of these samples were
199 subsequently prepared for OSL dating (XBMY-OSL-1, -2, -3 and -5), of which XBMY-
200 OSL-1 was collected from the cultural layer (Layer 5).

201 OSL dating

202 Over the last 30 years, OSL dating has become one of the most widely
203 used numerical dating methods to determine burial ages for Quaternary sediments in
204 variety of depositional environments (Huntley et al., 1985; Aitken, 1998; Lian and
205 Roberts, 2006; Jacobs and Roberts, 2007; Preusser, 2008; Rhodes, 2011; Wintle,
206 2014; Roberts et al., 2015). The method determines the time elapsed since common
207 minerals, such as quartz and potassium feldspar (K-feldspar), were last exposed to
208 light or heat (temperatures above ~ 300 °C). Exposure to sunlight empties the light-
209 sensitive electron 'traps' in these minerals, and these traps then steadily refill with
210 electrons while the mineral grains are buried in the ground, where they are shielded

211 from sunlight and exposed to background levels of ionising radiation. In the
212 laboratory, the grains are exposed to green or blue light, which causes the light-
213 sensitive electrons to escape from their traps and their subsequent recombination at
214 luminescence centres results in the emission of photons (i.e., OSL).

215 The burial time of a mineral grain can be estimated from the intensity of this
216 OSL signal, by converting it into a dose equivalent (D_e) and dividing the D_e by the
217 environmental dose rate. The latter represents the rate of supply of ionising radiation
218 to the grain over the period of burial from environmental sources of alpha, beta and
219 gamma radiation (due to the decay of radionuclides in the uranium and thorium
220 decay chains and ^{40}K) and from cosmic rays.

221 *Sample collection, preparation and dose rate determination*

222 Block samples about 10x10x10 cm in size were collected from the cleaned
223 section faces. After the blocks were removed, they were immediately wrapped in
224 light-proof plastic and transported to the Luminescence Dating Laboratory at the
225 University of Wollongong for preparation and analysis. In the laboratory, the outer
226 layer (~2 cm) of the blocks was removed under subdued red light and the materials
227 from the outer layer were used for dose rate determination. Quartz grains were
228 extracted from each of the trimmed blocks using standard mineral separation
229 procedures (Aitken, 1998). Carbonate and organic matter were removed using HCl
230 and H_2O_2 solutions, respectively, and quartz grains of 125–150 μm in diameter were
231 isolated by wet sieving and density separation (2.62 and 2.70 g/cm^3). These grains
232 were then etched in 40% HF acid for 40 min to dissolve any remaining feldspar
233 grains and to remove the alpha-irradiated outer layer of each quartz grain. The
234 etched quartz grains were then washed in HCl solution to remove any precipitated
235 fluorides.

236 For dose rate determinations, the beta dose rates were measured directly using
237 a low-level beta counter (Bøtter-Jensen and Mejdahl, 1988; Jacobs and Roberts,
238 2015) and the gamma dose rates were calculated from the U and Th contents
239 determined by thick-source alpha counting (Aitken, 1985) and the K contents
240 measured by X-ray fluorescence spectroscopy. Cosmic-ray dose rates were
241 estimated from the burial depth of each sample and the latitude, longitude and
242 altitude of Xibaimaying (Prescott and Hutton, 1994). As the sampled section at this
243 site has been aurally exposed for a prolonged period since excavation, it is likely to
244 have dried out considerably. Accordingly, we did not adjust the dry beta, gamma and
245 cosmic-ray dose rate using the measured (field) water contents, but instead used
246 water contents of $15 \pm 5\%$ for fluvial sample XBM-Y-OSL-1 and $10 \pm 3\%$ for samples
247 XBM-Y-OSL-2, 3 and 5 (probably aeolian or waterlain aeolian deposits), following
248 Guo et al. (2016). The calculated OSL ages increase (or decrease) by $\sim 1\%$ for each
249 1% increase (or decrease) in water content. A small, internal dose rate of 0.03 ± 0.01
250 Gy/ka due to U and Th inclusions within the quartz grains (e.g., Jacobs et al., 2008)
251 was included in the total environmental dose rate for each of the four samples.

252 *D_e determination*

253 OSL measurements were made on individual grains using standard single-grain
254 discs drilled with 100 holes, each 300 μm wide and 300 μm deep (Bøtter-Jensen et
255 al., 2000). Discs were checked under the microscope to verify that each hole
256 contained only one grain; this was true for most holes, but some contained two or
257 three grains. For the latter holes, the OSL signals should be derived predominantly
258 from only one grain, because $\sim 90\%$ of the total light sum for our samples originates
259 from the $\sim 11\%$ brightest grains (Figure S1). Thus, the OSL results for our samples
260 are considered representative of true single-grain analyses. Measurements were

261 performed on an automated Risø TL/OSL-DA-20 reader equipped with a calibrated
262 $^{90}\text{Sr}/^{90}\text{Y}$ beta source, a green (532 nm) laser for optical stimulation of individual
263 grains and blue light-emitting diodes (470 ± 30 nm) to stimulate single aliquots in the
264 preheat temperature test described below. The ultraviolet OSL emissions were
265 detected by an Electron Tubes Ltd 9235B photomultiplier fitted with Hoya U-340
266 filters.

267 D_e measurements were made using the single-aliquot regenerative-dose (SAR)
268 procedure (Murray and Roberts, 1998; Roberts et al., 1998a, 1998b; Galbraith et al.,
269 1999; Murray and Wintle, 2000, 2003; Wintle and Murray, 2006; Jacobs et al., 2006,
270 2008). In this procedure, the dose response curve (DRC) for each grain is
271 constructed using the sensitivity-corrected OSL signals (L_x/T_x) induced from a series
272 of regenerative doses, including a duplicate dose and a zero dose to monitor the
273 recycling ratio and the extent of recuperation, respectively. The D_e value of each
274 grain was obtained by interpolating the sensitivity-corrected natural OSL signal
275 (L_n/T_n) on to its corresponding DRC, which was fitted using a single saturating
276 exponential function, an exponential plus linear function, or the sum of two saturating
277 exponential functions—whichever provided the best fit to the L_x/T_x data. For each D_e
278 estimate, the associated uncertainty includes photon counting statistics, an
279 instrumental irreproducibility error of 2% for each OSL measurement (following
280 Jacobs et al., 2006), the curve fitting error, and the error involved in determining the
281 calibrated beta dose rate delivered to each grain position on a disc.

282 We also included an additional regenerative dose cycle at the end of the SAR
283 sequence (using an infrared stimulation for 40 s at 50 °C prior to measuring the OSL
284 signal) to determine the OSL IR depletion ratios and check for any remnant feldspar
285 contamination (Duller, 2003). Table S1b lists the full SAR measurement sequence

286 used for single grains in this study. The net OSL signals used for D_e estimation were
287 calculated as the sum of counts in the first 0.12 s of OSL decay minus a 'late light'
288 background estimated from the mean count rate over the final 0.12 s. Grains were
289 held for 0.1 s before and after optical stimulation to monitor and minimise any
290 interference from isothermal decay. A typical OSL decay curve and DRC is shown in
291 Fig. 4 for a single grain of quartz from sample XBMV-OSL-1.

292 To choose a suitable preheat temperature, we made D_e measurements on
293 single aliquots of sample XBMV-OSL-5 (where each aliquot consisted of ~200
294 grains) using the SAR procedure listed in Table S1a and preheat temperatures of
295 between 180 and 300 °C (step 2). Thirteen to twenty aliquots were measured at
296 each preheat temperature. The net OSL signal was determined as the sum of counts
297 in the first 0.64 s of OSL decay minus a background estimated from the mean count
298 rate over the final 3.2 s. The preheat given in step 5 after a fixed test dose (12.6 Gy)
299 was set 40 °C lower than that applied to the natural and regenerative doses; the sole
300 exception was the 180 °C preheat in step 2, which was accompanied by a preheat of
301 160 °C in step 5. At the end of each SAR cycle, a 'hot optical bleach' was performed
302 at a temperature 20 °C higher than the corresponding preheat in step 2, to erase any
303 remnant OSL signal. The weighted mean D_e values and the recycling and
304 recuperation ratios are plotted as a function of preheat temperature in Fig. 5. This
305 plot shows that a D_e 'plateau' (46 ± 3 Gy) is obtained at preheat temperatures of
306 220–260 °C and that the recycling ratios are consistent with unity at all preheat
307 temperatures (except 280 °C). This experiment indicates, therefore, that preheat
308 temperatures of between 220 and 260 °C should be suitable for determining D_e
309 values for the Xibaimaying samples.

310 A dose recovery test (Galbraith et al., 1999) was conducted using single grains
311 of quartz from sample XBMY-OSL-1. Measurement conditions included a natural and
312 regenerative dose preheat of 240 °C and a test dose preheat of 200 °C, based on
313 the preheat plateau test mentioned above. Two thousand grains were first bleached
314 for ~2 hr using a Dr Hönle solar simulator (Model: UVACUBE 400) and a dose of 140
315 Gy was then given to the bleached grains as the surrogate 'natural' dose. The grains
316 were measured using the procedures listed in Table S1b, with the test dose fixed at
317 30 Gy. Grains were rejected if the resulting OSL data failed to satisfy a series of well-
318 established criteria similar to those proposed by Jacobs et al. (2006), namely if: 1)
319 the initial T_n signal was less than 3 times its corresponding background or its relative
320 error was greater than 25%; 2) the recuperation ratio was larger than 10%; 3) the
321 recycling ratio or OSL IR depletion ratio differed from unity by more than 2σ ; 4) the
322 DRC provided an obviously poor fit to the L_x/T_x data points; and 5) the L_n/T_n value
323 was consistent with or exceeded the saturation level of the corresponding DRC. The
324 number of grains rejected according to each of these criteria are summarised (in
325 order of rejection) in Table S2.

326 A total of 122 grains (6% of the 2000 grains measured) were accepted for dose
327 determination after applying these rejection criteria. The distribution of the dose
328 recovery ratios (i.e., ratios of measured to given dose) for all accepted grains is
329 shown in Fig. 6a. The over-dispersion (OD) value for this dose distribution,
330 calculated using the Central Age Model (CAM: Galbraith et al., 1999; Galbraith and
331 Roberts, 2012) is $23.5 \pm 2.9 \%$ and the weighted mean ratio is 0.90 ± 0.03 (also
332 calculated using the CAM). The latter value is slightly less than unity and indicates
333 that the given dose was not recovered fully using the measurement conditions and/or
334 the data selection criteria.

335 Li et al. (2016) have suggested that if a significant proportion of grains in a
336 sample yield infinite D_e values (i.e., L_n/T_n values in the saturated region of the DRC),
337 then this could result in a truncated D_e distribution and a corresponding
338 underestimation of true D_e and age. They suggested that a more reliable estimate of
339 D_e could be obtained based on those grains that saturate at larger doses. Rejection
340 of quartz grains with low characteristic saturation doses (D_0 values) has been used
341 previously in single-grain OSL dating to improve the accuracy of the resulting D_e
342 estimates (e.g., Duller, 2012; Gliganic et al., 2012). We hypothesised, therefore, that
343 underestimation of the applied dose in the dose recovery test may be due to the
344 given dose (140 Gy) lying at or close to the saturation level of a significant proportion
345 of the measured grains.

346 To test this hypothesis, after applying the first 4 rejection criteria mentioned
347 above, we sorted the accepted grains according to their D_0 values, which we
348 calculated from the DRCs fitted to the L_x/T_x data points using a single saturating
349 exponential function; the latter has the form $I = I_0(1 - e^{-D/D_0}) + c$, where I is the
350 sensitivity-corrected OSL intensity, D is the regenerative dose, and I_0 and c are
351 constants. We then applied the fifth rejection criterion to recalculate the recovered
352 dose (using the CAM) while increasing the minimum D_0 threshold from 0 to 300 Gy
353 in steps of 30 Gy. The CAM dose estimates, OD values and the numbers of
354 accepted and saturated grains at different minimum D_0 thresholds are summarised in
355 Table S3, and the corresponding dose recovery ratios are plotted in Fig. 6b. The
356 dose recovery ratios increase in concert with the D_0 threshold, achieving values
357 consistent with unity at a D_0 threshold of 90 Gy and above.

358 We then scrutinised these data further to identify the D_0 threshold at which the
359 number of the saturated grains reached zero (Table S3); we define this value as the

360 'optimum- D_0 threshold'. For the dose recovery test, the optimum- D_0 threshold is 120
361 Gy—resulting in a dose recovery ratio of 0.97 ± 0.04 (Fig. 6b), which is consistent
362 with unity (Table S3). For the single-grain measurements of the older samples from
363 Xibaimaying, therefore, it would appear necessary to first sort the accepted grains
364 according to their grain-specific D_0 values and then determine the optimum- D_0
365 threshold to avoid truncating the upper end of the single-grain D_e distribution.

366 The preheat temperature test on sample XBMY-OSL-5 and the dose recovery
367 test and D_0 -threshold procedure applied to sample XBMY-OSL-1 have yielded a set
368 of SAR measurement conditions and data analysis procedures that should be
369 suitable for dating the Xibaimaying samples. We measured a total of 3400, 2800,
370 1400 and 1900 grains of samples XBMY-OSL-1, -2, -3 and -5, respectively, using the
371 procedures in Table S1b; the test dose was fixed at 30 Gy for samples XBMY-OSL-
372 1, -2 and -3 and 10 Gy for sample XBMY-OSL-5. Of the measured grains, 135, 141,
373 71 and 82 were accepted for samples XBMY-OSL-1, -2, -3 and -5, respectively, after
374 applying the 5 rejection criteria described above (Table S2). The D_e values for these
375 grains are displayed in Fig. 7. Note that these D_e estimates were obtained before
376 applying the optimum- D_0 threshold criterion, so that we could evaluate its
377 subsequent effect on the D_e distributions.

378 Samples XBMY-OSL-1, -2, -3 and -5 each contained some saturated grains,
379 amounting to approximately 29, 29, 13 and 3% of the total number of accepted
380 grains, respectively (Table S2). The CAM D_e values of samples XBMY-OSL-1 and -
381 2, in particular, are thus potentially underestimated, owing to the high proportion
382 (>20%) of saturated grains. After applying the first 4 rejection criteria mentioned
383 above, we then sorted the accepted grains by the D_0 values of their DRCs. The
384 corresponding recalculated CAM D_e values are plotted as a function of D_0 threshold

385 in Fig. 8; the optimum- D_0 threshold values are 120, 150, 120 and 30 Gy for samples
386 XBM-Y-OSL-1, -2, -3 and -5, respectively (Table S3). For samples XBM-Y-OSL-1 and
387 -2, the CAM D_e estimates attain a 'plateau' close to and above the optimum- D_0
388 threshold value (zero saturated grains), while the CAM D_e values are statistically
389 consistent for all D_0 thresholds for samples XBM-Y-OSL-3 and -5 due to less
390 saturated grains (< 13 %) in the latter two samples. The D_e estimates for grains with
391 D_0 values at or above the optimum thresholds are displayed as solid triangles in Fig.
392 7. The OD values for these samples are reduced from 46–50% to 35–42% after
393 applying the optimum- D_0 threshold criterion, and the D_e values appear to be
394 randomly distributed around a central value. We calculated the final D_e estimates
395 using the CAM, which yielded values of 147.2 ± 7.5 , 112.4 ± 6.5 , 82.7 ± 7.5 and 39.3
396 ± 2.5 Gy for samples XBM-Y-OSL-1, -2, -3 and -5, respectively. We note that the
397 single-grain D_e value for sample XBM-Y-OSL-1 (39.3 ± 2.5 Gy) is consistent at 2σ
398 with its single-aliquot D_e 'plateau' value (46 ± 3 Gy).

399 Ages and implications

400 Table 1 summarises the dose rates, D_e values and OSL ages for the four
401 samples from Xibaimaying. The ages are in correct stratigraphic order (Fig. 2d),
402 increasing down-profile from early Holocene in Layer 2 (13 ± 1 ka: XBM-Y-OSL-5) to
403 early MIS 2 or late MIS 3 in the middle and lower parts of Layer 4 (24 ± 2 and 32 ± 2
404 ka: XBM-Y-OSL-3 and -2, respectively), with the basal, artefact-bearing sediments
405 (Layer 5) deposited in mid-MIS 3 (46 ± 3 ka: XBM-Y-OSL-1). The latter age is
406 consistent with a recent ^{14}C age determination of 47–50 ka cal BP for a fragment of
407 ostrich eggshell recovered from the cultural layer at this site (Ying Guan, Institute of
408 Vertebrate Paleontology and Paleoanthropology, personal communication). The
409 coherent stratigraphic ordering of OSL ages, and the agreement with the ^{14}C age

410 determination for the cultural layer, supports the reliability of our chronology. These
411 results also suggest that the uranium-series ages of 18 ± 1 and 15 ± 1 ka obtained
412 from bovid teeth (Xie and Yu, 1989) should be viewed as minimum estimates of age,
413 as might be expected for such materials given their open-system geochemical
414 behaviour (Grün et al., 2014).

415 The age of 46 ± 3 ka for the cultural layer potentially falls within the 43–51 ka
416 period of MIS 3 during which the local landscape was indicated covered by sparse
417 desert-steppe vegetation in lowland areas and the northern Loess Plateau, merging
418 into a mixture of steppe and coniferous forest in the surrounding highlands (Liu et al.,
419 2014). The pollen and spore composition has also been examined for the cultural
420 layer at the site, and this also indicates a sparse coniferous forest and desert steppe
421 vegetation (Xie and Yu, 1989): herbs (mainly *Artemisia*) account for 93.4% of the
422 pollen and spores, with trees (mostly *Pinus* and *Picea*) and ferns accounting for only
423 4.4% and 2.2%, respectively.

424 As mentioned above, it has long been regarded by Chinese archaeologists that
425 the small-tool and microblade industries coexisted without mutual influence in the
426 Nihewan Basin, based largely on the uranium-series ages for Xibaimaying (Xie and
427 Yu, 1989; Xie et al., 2006; Liu et al., 2013; Jia et al., 2015). Our OSL chronology for
428 this site shows that the small-tool artefacts are 14–25 ka older than the microblade
429 artefacts found at the Youfang site (26–29 ka), which are the earliest known
430 occurrence of typical microblade tools in the Nihewan Basin. The ages of the
431 artefacts at Xibaimaying are also older than those at the Zhiyu site (~31–39 ka cal
432 BP), which are considered by some archaeologists (e.g., Jia et al., 1972; Jia, 1978)
433 to exhibit ‘transitional’ traits between small-tool and microblade technologies. The
434 new ages reported here, therefore, are compatible with a developmental trend in

435 stone tool technology in the Nihewan Basin from mid-MIS 3 to early MIS 2, from
436 small-tool technology (Xibaimaying) to ‘transitional’ small-tool/microblade artefacts
437 (Zhiyu) to typical microblade technology (Youfang). Fig. 9 provides a graphical
438 summary of the existing and new chronologies for the different technologies in the
439 basin.

440 The origin of the microblade technology in North China has been the subject of
441 considerable debate over the past few decades, as summarised in the reviews by
442 Zhu (2006: 130–135) and Yi et al. (2016). There are two general hypotheses: this
443 technology emerged in situ from the local small-tool tradition (e.g., Jia et al., 1972;
444 Jia, 1978) or was introduced from northern Siberia or Mongolia (e.g., Keates, 2007;
445 Kuzmin, 2007). The first hypothesis is based on discoveries of ‘microblade traits’ at
446 some local small-tool sites (e.g., the ‘Donggutuo Core’); whereas the second
447 hypothesis argued that the microblades were not “simply a type of small tool”, but
448 “stand for products of a special technology including microblades, microblade cores,
449 and tools made with microblades”, and this hypothesis has received support from the
450 chronological sequence of microblade sites in Siberia, Mongolia and North China (Yi
451 et al., 2016: 131). Microblade artefacts appear in Siberia as early as ~35 ka
452 (Derevianko et al., 1998) and the earliest known sites in China with typical
453 microblade artefacts are Longwangchan and Youfang (Fig. 1), which have been
454 dated by OSL to 25–29 ka (Zhang et al., 2011) and 26–29 ka (Nian et al., 2014),
455 respectively.

456 Our OSL dating results for Xibaimaying are consistent with the small-tool
457 industry preceding the microblade industry in the Nihewan Basin and, thus, lend
458 support to the ‘local origin’ hypothesis for microblade technology. But in the absence
459 of independent evidence for the identity of the toolmakers, we cannot discount the

460 possibility that the technology was introduced by people migrating from northern
461 Siberia or Mongolia. Furthermore, an issue with the study of the origins of the
462 microblade in North China is that many Chinese archaeologists have focussed on
463 artefacts found in northeast Asia. Microblade tools have been reported from earlier
464 contexts in other parts of the world, such as ~71 ka in South Africa (Brown et al.,
465 2012) and ~48 ka in India (Mishra et al., 2013; Basak et al., 2014), so a southern
466 origin for this technology should also be taken into consideration. The key to
467 revealing the origin of the microblade in North China will be to establish reliable
468 spatial and temporal distribution patterns for this technology not only in northeast
469 Asia but also throughout East and South Asia.

470 Conclusions

471 In this study, we have re-dated the 'latest' small-tool industry site (Xibaimaying)
472 in the Nihewan Basin using single-grain OSL methods for quartz. Our chronology
473 indicates that the cultural layer was deposited 46 ± 3 ka ago, corresponding to the
474 middle of MIS 3, rather than the later part of MIS 2 as suggested previously by
475 uranium-series dating of bovid teeth (Xie and Yu, 1989). A developmental trend in
476 artefact technology is one inference from our data—that is, a change from the small-
477 tool industry at Xibaimaying (46 ± 3 ka) to the earliest microblade at Zhiyu (31–39 ka
478 cal BP) and the typical microblade at Youfang (26–29 ka). This pattern contrasts with
479 the parallel development of these two lithic technologies in the basin during the
480 Upper Palaeolithic (Fig. 9), which is the prevailing view among many archaeologists.
481 However, until further archaeological and chronological studies are conducted on
482 Late Pleistocene sites containing small-tool and microblade artefacts in northern
483 China—and in other parts of Asia—we cannot be certain of the temporal relation

484 between these two industries or the geographic origin of the local microblade
485 technology.

486 Acknowledgements

487 This study was supported by postgraduate scholarships from the China
488 Scholarship Council and the University of Wollongong to Y.G. (201206010053), an
489 Australian Research Council Future Fellowship to B.L. (FT140100384), a grant from
490 the National Natural Science Foundation of China to J.Z. (NSFC, No. 41471003),
491 and an Australian Research Council Australian Laureate Fellowship to R.G.R.
492 (FL130100116). We thank Weiwen Huang, Yue Hu, Yongmin Meng, Qi Wei,
493 Shengquan Cheng, Fagang Wang, Yang Liu and others who helped with the field
494 investigations and collection of OSL samples and relevant literature.

495 Supporting Information

496 Additional supporting information is available in the online version of this article.

497 Figure S1. The single-grain 'brightness' distribution for 200 individual grains of
498 sample XBMY-OSL-1. The cumulative light sum of the L_n signals (shown on the y -
499 axis) is plotted as a function of the corresponding proportion of grains (shown on the
500 x -axis).

501 Table S1. Single-aliquot regenerative-dose (SAR) procedures used in this study.

502 Table S2. Numbers of single grains measured, rejected and accepted for D_e
503 determination.

504 Table S3. Numbers of accepted and saturated grains at various D_0 thresholds, and
505 corresponding CAM and OD values.

506 **References**

- 507 Aitken MJ. 1985. *Thermoluminescence Dating*. Academic Press: London.
- 508 Aitken MJ. 1998. *An Introduction to Optical Dating*. Oxford University Press: Oxford.
- 509 An ZM. 1965. Trial excavation of the Paleolithic cave of Hsiao-nan-hai in Anyang,
510 Honan (in Chinese). *Acta Archaeologica Sinica* 1: 1–26.
- 511 Basak B, Srivastava P, Dasgupta S, Kumar A, Rajaguru SN. 2014. Earliest dates
512 and implications of microlithic industries of Late Pleistocene from Mahadebbera
513 and Kana, Purulia district, West Bengal. *Current Science* 107: 1167–1171.
- 514 Bøtter-Jensen L, Bulur E, Duller GAT, Murray AS. 2000. Advances in luminescence
515 instrument systems. *Radiation Measurements* 32: 523–528.
- 516 Bøtter-Jensen L, Mejdahl V. 1988. Assessment of beta dose rate using a GM
517 multicounter system. *Nuclear Tracks and Radiation Measurements* 14: 187–191.
- 518 Brown KS, Marean CW, Jacobs Z, Schoville BJ, Oestmo S, Fisher EC, Bernatchez
519 J, Karkanas P, Matthews T. 2012. An early and enduring advanced technology
520 originating 71,000 years ago in South Africa. *Nature* 491: 590–593.
- 521 Chen, C. 1984. The microlithic in China. *Journal of Anthropological Archaeology* 3:
522 79–115.
- 523 Derevianko AP. 2001. The Middle to Upper Palaeolithic transition in the Altai
524 (Mongolia and Siberia). *Archaeology, Ethnology and Anthropology of Eurasia* 3:
525 70–103.
- 526 Derevianko AP, Agadzhanian AK, Baryshnikov GF, Dergacheva MI, Dupal TA,
527 Malaeva EM, Markin SV, Molodin VI, Nikolaev SV, Orlova LA, Petrin VT, Postnov

- 528 AV, Ul'ianov VA, Fedeneva IN, Foronova IV, Shun'kov MV. 1998. *Arkheologiya,*
529 *geologiya i paleogeografiya pleistozena i golozena Gornogo Altaya (Archaeology,*
530 *Geology, and Paleogeography of the Pleistocene and Holocene of the*
531 *Mountainous Altai)* (in Russian). Institute of Archaeology and Ethnography Press:
532 Novosibirsk.
- 533 Duller GAT. 2003. Distinguishing quartz and feldspar in single grain luminescence
534 measurements. *Radiation Measurements* 37: 161–165.
- 535 Duller GAT. 2012. Improving the accuracy and precision of equivalent doses
536 determined using the optically stimulated luminescence signal from single grains
537 of quartz. *Radiation Measurements* 47: 770–777.
- 538 Du SS. 2003. A preliminary study on raw material exploitation in Middle–Upper
539 Palaeolithic sites in Nihewan Basin (in Chinese with English abstract). *Acta*
540 *Anthropologica Sinica* 22: 121–130.
- 541 Gai P. 1991. Microblade tradition around the northern Pacific rim: a Chinese
542 Perspective. In *Proceedings of the XIII International Quaternary Conference,*
543 *Institute of Vertebrate Palaeontology and Palaeoanthropology* (ed). Scientific and
544 *Technological Publishing House: Beijing; 21–31.*
- 545 Galbraith RF, Roberts RG, Laslett GM, Yoshida H, Olley JM. 1999. Optical dating of
546 single and multiple grains of quartz from Jinmium rock shelter, northern Australia:
547 Part I, experimental design and statistical models. *Archaeometry* 41: 339–364.
- 548 Galbraith RF, Roberts RG. 2012. Statistical aspects of equivalent dose and error
549 calculation and display in OSL dating: an overview and some recommendations.
550 *Quaternary Geochronology* 11: 1–27.

- 551 Gliganic LA, Jacobs Z, Roberts RG. 2012. Luminescence characteristics and dose
552 distributions for quartz and feldspar grains from Mumba rockshelter, Tanzania.
553 *Archaeological and Anthropological Sciences* 4: 115–135.
- 554 Grün R, Eggins S, Kinsley L, Moseley H, Sambridge M. 2014. Laser ablation U-
555 series analysis of fossil bones and teeth. *Palaeogeography, Palaeoclimatology,*
556 *Palaeoecology* 416: 150–167.
- 557 Guo YJ, Li B, Zhang JF, Roberts RG. 2015. Luminescence-based chronologies for
558 Palaeolithic sites in the Nihewan Basin, northern China: First tests using newly
559 developed optical dating procedures for potassium feldspar grains. *Journal of*
560 *Archaeological Science: Reports* 3: 31–40.
- 561 Guo YJ, Li B, Zhang JF, Yuan BY, Xie F, Roberts, RG. 2016. Luminescence ages for
562 three ‘Middle Palaeolithic’ sites in the Nihewan Basin, northern China, and their
563 archaeological and palaeoenvironmental implications. *Quaternary Research* 85:
564 456–470.
- 565 Han F, Bahain JJ, Boëda É, Hou Y, Huang W, Falguères C, Rasse M, Wei G, Garcia
566 T, Shao Q, Yin G. 2012. Preliminary results of combined ESR/U-series dating of
567 fossil teeth from Longgupo cave, China. *Quaternary Geochronology* 10: 436–442.
- 568 Hellstrom J, Pickering R. 2015. Recent advances and future prospects of the U–Th
569 and U–Pb chronometers applicable to archaeology. *Journal of Archaeological*
570 *Science* 56: 32–40.
- 571 Hou YM. 2008. The “Donggutuo core” from Donggutuo industry of Lower Pleistocene
572 in the Nihewan Basin, North China and its indication. *L’Anthropologie* 112: 457–
573 471.

- 574 Hou YM, Liu Y, Li YH, Liu H. 2010. A report on the 2008 test excavation at the
575 Sankeshu Paleolithic site in the Nihewan Basin (in Chinese with English abstract).
576 *Acta Anthropologica Sinica* 29: 227–241.
- 577 Hou YM, Wei Q, Feng XW, Lin SL. 1999. Re-excavation at Donggutuo in the
578 Nihewan Basin, North China (in Chinese with English abstract). *Quaternary*
579 *Sciences* 2: 139–147.
- 580 Hou YM. 2003. Naming and preliminary study on the category of the “Donggutuo
581 core” (in Chinese with English abstract). *Acta Anthropologica Sinica* 22: 279–292.
- 582 Hou YM. 2005. Shuidonggou: A vane of intercommunication between the East and
583 the West? —Discussion about Small Tool Culture in North China and hypothesis
584 of the “Lithic Road” (in Chinese with English abstract). *Quaternary Sciences* 25:
585 750–761.
- 586 Huang WW. 1964. On a collection of Paleoliths from Sanmen area in western Honan
587 (in Chinese with English abstract). *Vertebrate PalAsiatica* 8: 162–177.
- 588 Huntley DJ, Godfrey-Smith DI, Thewalt MLW. 1985. Optical dating of sediments.
589 *Nature* 313: 105–107.
- 590 Institute of Archaeology of Chinese Academy of Social Sciences. 1991. Radiocarbon
591 dates in Chinese Archaeology (1965–1991) (in Chinese). Kaoguxuezhuan 28.
592 Culture Relic Press: Beijing.
- 593 Institute of Archaeology of Northern Ethnicity and Department of Archaeology and
594 Museology, Renmin University. 2006. *The Archaeology of Northern Ethnicity* (in
595 Chinese). Science Press: Beijing.

- 596 Jacobs Z, Roberts RG. 2007. Advances in optically stimulated luminescence dating
597 of individual grains of quartz from archeological deposits. *Evolutionary*
598 *Anthropology* 16: 210–223.
- 599 Jacobs Z, Roberts RG. 2015. An improved single grain OSL chronology for the
600 sedimentary deposits from Diepkloof Rockshelter, Western Cape, South Africa.
601 *Journal of Archaeological Science* 63: 175–192.
- 602 Jacobs Z, Duller GA, Wintle AG. 2006. Interpretation of single grain D_e distributions
603 and calculation of D_e . *Radiation Measurements* 41: 264–277.
- 604 Jacobs Z, Wintle AG, Duller GAT, Roberts RG, Wadley L. 2008. New ages for the
605 post-Howiesons Poort, late and final Middle Stone Age at Sibudu, South Africa.
606 *Journal of Archaeological Science* 35: 1790–1807.
- 607 Jia LP, Gai P, You YZ. 1972. Report on the excavation at Zhiyu Paleolithic site in
608 Shanxi Province (in Chinese). *Kaoguxuebao* 1: 39–58.
- 609 Jia LP, Wei T, Wang J. 1961. The Palaeolithic site of Kehe in Ruicheng, Shanxi
610 province (in Chinese). *Archaeology* 8: 395–397.
- 611 Jia LP, You YZ. 1973. Emaokou stone tool workshop in Huaiaren. Shanxi (in
612 Chinese). *Kaoguxuebao* 2: 13–26.
- 613 Jia LP. 1978. The feature of microlithic and its tradition, origin in China (in Chinese
614 with English abstract). *Vertebrata PalAsiatica* 16: 137–143.
- 615 Jia ZX, Zhang XL, Pei SW. 2015. Stone artifacts collected from the Xibaimaying site
616 in the Nihewan Basin (in Chinese). *Acta Anthropologica Sinica* 34: 299–306.
- 617 Keates SG. 2007. Microblade technology in Siberia and neighboring regions: an
618 overview. In *Origin and Spread of Microblade Technology in Northern Asia and*

- 619 *North America*, Kuzmin YV, Keates SG, Chen S (eds.). Archaeology Press: Simon
620 Fraser University: Burnaby; 125–146.
- 621 Kuzmin YV. 2007. Geoarchaeological aspects of the origin and spread of microblade
622 technology in northern and central Asia. In *Origin and Spread of Microblade*
623 *Technology in Northern Asia and North America*, Kuzmin YV, Keates SG, Chen S.
624 (eds.). Archaeology Press: Simon Fraser University, Burnaby; 115–124.
- 625 Li B, Jacobs Z, Roberts RG. 2016. Investigation of the applicability of standardised
626 growth curves for OSL dating of quartz from Haua Fteah cave, Libya. *Quaternary*
627 *Geochronology* 35, 1–15.
- 628 Lian OB, Roberts RG. 2006. Dating the Quaternary: progress in luminescence dating
629 of sediments. *Quaternary Science Reviews* 25: 2449–2468.
- 630 Lisiecki, LE, Raymo ME. 2005. A Pliocene-Pleistocene stack of 57 globally
631 distributed benthic $\delta^{18}\text{O}$ records. *Paleoceanography* 20: PA1003.
- 632 Liu X, Chi Z, Herzsuh U, Wang Y, Ni J, Xu Q. 2014. A MIS 3 charcoal and pollen
633 record and quantitative precipitation inferences from the Jingerwa section of the
634 Nihewan Basin, north-central China. *Journal of Paleolimnology* 51: 211–221.
- 635 Liu Y. 2014. The origin and developmental road of the small tool technology in
636 northern China (in Chinese). *Wenwuchunqiu* 2: 3–13.
- 637 Liu Y, Hu YM, Wei Q. 2013. Early to Late Pleistocene human settlements and the
638 evolution of lithic technology in the Nihewan Basin, North China: a macroscopic
639 perspective. *Quaternary International* 295: 204–214.

640 Mishra S, Chauhan N, Singhvi AK. 2013. Continuity of microblade technology in the
641 Indian subcontinent since 45 ka: implications for the dispersal of modern humans.
642 *PLoS ONE* 8(7): e69280.

643 Mu H, Xu Q, Zhang S, Hun L, Li M, Li Y, Hu Y, Xie F. 2015. Pollen-based
644 quantitative reconstruction of the paleoclimate during the formation process of
645 Houjiayao Relic Site in Nihewan Basin of China. *Quaternary International* 374:
646 76–84.

647 Murray AS, Roberts RG. 1998. Measurement of the equivalent dose in quartz using
648 a regenerative-dose single-aliquot protocol. *Radiation Measurements* 29: 503–
649 515.

650 Murray AS, Wintle AG. 2000. Luminescence dating of quartz using an improved
651 single-aliquot regenerative-dose protocol. *Radiation Measurements* 32: 57–73.

652 Murray AS, Wintle AG. 2003. The single-aliquot regenerative-dose protocol: potential
653 for improvements in reliability. *Radiation Measurements* 37: 377–381.

654 Nian XM, Gao X, Xie F, Mei HJ, Zhou LP. 2014. Chronology of the Youfang site and
655 its implications for the emergence of microblade technology in North China.
656 *Quaternary International* 347: 113–121.

657 Norton CJ, Gao X. 2008. Hominin–carnivore interactions during the Chinese Early
658 Paleolithic: Taphonomic perspectives from Xujiayao. *Journal of Human Evolution*
659 55: 164–178.

660 Preusser F, Degering D, Fuchs M, Hilgers A, Kadereit A, Klasen N, Krbetschek M,
661 Richter D, Spencer JQ. 2008. Luminescence dating: basics, methods and
662 applications. *Eiszeitalter und Gegenwart* 57: 95–149.

663 Prescott JR, Hutton JT. 1994. Cosmic ray contributions to dose rates for
664 luminescence and ESR dating: large depths and long-term time variations.
665 *Radiation Measurements* 23: 497–500.

666 Rhodes EJ. 2011. Optically stimulated luminescence dating of sediments over the
667 past 200,000 years. *Annual Review of Earth and Planetary Sciences* 39: 461–488.

668 Roberts RG, Jacobs Z, Li B, Jankowski NR, Cunningham AC, Rosenfeld AB. 2015.
669 Optical dating in archaeology: thirty years in retrospect and grand challenges for
670 the future. *Journal of Archaeological Science* 56: 41–60.

671 Roberts RG, Bird M, Olley J, Galbraith R, Lawson E, Laslett G, Yoshida H, Jones R,
672 Fullagar R, Jacobsen G, Hua Q. 1998a. Optical and radiocarbon dating at
673 Jinmium rock shelter in northern Australia. *Nature* 393: 358–362.

674 Roberts R, Yoshida H, Galbraith R, Laslett G, Jones R, Smith M. 1998b. Single-
675 aliquot and single-grain optical dating confirm thermoluminescence age estimates
676 at Malakunanja II rock shelter in northern Australia. *Ancient TL* 16: 19–24.

677 Schick K, Toth N, Qi W, Clark JD, Etler D. 1991. Archaeological perspectives in the
678 Nihewan Basin, China. *Journal of Human Evolution* 21: 13–26.

679 Teilhard de Chardin P, Pei WG. 1932. The lithic industry of the Sinanthropus deposits
680 in Choukoutien. *Bulletin of the Geological Society of China* 11: 315–364.

681 Teilhard de Chardin TD, Licent F. 1924. On the discovery of a Palaeolithic industry in
682 northern China. *Bulletin of the Geological Society of China* 3: 45–50.

683 Tu H, Shen GJ, Li HX, Xie F, Granger DE. 2015. $^{26}\text{Al}/^{10}\text{Be}$ Burial Dating of Xujiayao-
684 Houjiayao Site in Nihewan Basin, Northern China. *PLoS ONE* 10(2): e0118315.

- 685 Wang H, Deng C, Zhu R, Wei Q, Hou Y, Boëda E. 2005. Magnetostratigraphic dating
686 of the Donggutuo and Maliang Paleolithic sites in the Nihewan Basin, North China.
687 *Quaternary Research* 64: 1–11.
- 688 Wang YP. 2006. *Stone Artefacts Studies: Explorations of the Palaeolithic*
689 *Archaeological Methods* (in Chinese). Peking University Press: Beijing.
- 690 Wei Q. 2004. The Paleolithic of Nihewan Basin (in Chinese). In *Review of China's*
691 *Century of Archaeological Research (Paleolithic Archaeology)*, Lu ZE (ed).
692 Science Press: Beijing; 84–110.
- 693 Wei Q, Pei SW, Jia ZX, Chi ZQ, Wang Y. 2016. Heitugou Paleolithic site from the
694 Lower Pleistocene in the Nihewan Basin, northern China (in Chinese with
695 English abstract). *Acta Anthropologica Sinica* 35: 43–62.
- 696 Wintle AG. 2014. Luminescence dating methods. In *Treatise on Geochemistry (2nd*
697 *edition)*, Holland H, Turekian K (eds.). Elsevier: Oxford; 17–35.
- 698 Wintle AG, Murray AS. 2006. A review of quartz optically stimulated luminescence
699 characteristics and their relevance in single-aliquot regeneration dating protocols.
700 *Radiation Measurements* 41: 369–391.
- 701 Xia ZK, Chen FY, Chen G, Zheng GW, Xie F, Mei HJ. 2001. Environmental
702 background of evolution from the Paleolithic to Neolithic culture in Nihewan Basin,
703 North China. *Science in China Series D: Earth Sciences* 44: 779–788.
- 704 Xie F, Li J, Liu LQ. 2006. *Paleolithic Archeology in the Nihewan Basin* (in Chinese).
705 Huashan Literature and Arts Press: Shijiazhuang.
- 706 Xie F, Yu SF. 1989. A study of Paleolithic remains from Xibaimaying, Yangyuan,
707 Hebei (in Chinese with English abstract). *Wenwu Chunqiu* 3: 13–26.

- 708 Yi MJ, Gao X, Li F, Chen F. 2016. Rethinking the origin of microblade technology: A
709 chronological and ecological perspective. *Quaternary International* 400: 130–139.
- 710 Yuan SX. 1993. AMS radiocarbon dating of Xinglong carved antler, Shiyu and
711 Ximiao sites (in Chinese with English abstract). *Acta Anthropologica Sinica* 12: 92–
712 95.
- 713 Zhang CC, Li L, Wang J, Xu QH, Huang HF. 2015. Research on the relationship
714 between the old river and living environment for ancient human at Houjiayao site,
715 Yangyuan County, Hebei Province (in Chinese with English abstract). *Quaternary*
716 *Sciences* 35: 733–741.
- 717 Zhang JF, Wang XQ, Qiu WL, Shelach G, Hu G, Fu X, Zhuang MG, Zhou LP. 2011.
718 The paleolithic site of Longwangchan in the middle Yellow River, China:
719 chronology, paleoenvironment and implications. *Journal of Archaeological*
720 *Science* 38: 1537–1550.
- 721 Zhang SS. 1990. Regional industrial gradual advance and cultural exchange of
722 Paleolithic in North China (in Chinese with English abstract). *Acta Anthropologica*
723 *Sinica* 9: 322–333.
- 724 Zhang SS. 1999. On the important advancements of the Palaeolithic archeology in
725 China since 1949 (in Chinese with English abstract). *Acta Anthropologica Sinica*
726 18: 193–214.
- 727 Zhao H, Lu Y, Wang C, Chen J, Liu J, Mao H. 2010. ReOSL dating of aeolian and
728 fluvial sediments from Nihewan Basin, northern China and its environmental
729 application. *Quaternary Geochronology* 5: 159–163.

- 730 Zhu RX, Hoffman KA, Potts R, Deng CL, Pan YX, Guo B, Shi CD, Guo ZT, Yuan BY,
731 Hou YM, Huang WW. 2001. Earliest presence of humans in northeast Asia.
732 *Nature* 413: 413–417.
- 733 Zhu RX, Potts R, Xie F, Hoffman KA, Deng CL, Shi CD, Pan YX, Wang HQ, Shi RP,
734 Wang YC, Shi GH. 2004. New evidence on the earliest human presence at high
735 northern latitudes in northeast Asia. *Nature* 431: 559–562.
- 736 Zhu ZY. 2006. The study on lithic assemblage from the Hutouliang site in North
737 China (in Chinese with English abstract). PhD thesis, Institute of Vertebrate
738 Paleontology and Paleoanthropology, Chinese Academy of Sciences: Beijing.

739 Figure captions

740 Fig. 1: (a) Map of China showing the Palaeolithic sites mentioned in this study
741 (modified after Han et al., 2012). Triangles and circles represent small-tool and
742 microlithic sites, respectively. (b) Map of the Nihewan Basin showing the Palaeolithic
743 sites mentioned in this study (modified after Wei, 2004). Zhiyu has artefacts
744 'transitional' between small-tool and microlithic technologies (Jia et al., 1972; Jia,
745 1978).

746 Fig. 2: (a) Photo looking northwest, showing the location of the Xibaimaying site on
747 the east bank of the Nangou gully. (b) Sedimentary profile of the excavated east
748 face, showing locations of the OSL samples. (c) Animal remains in the cultural layer,
749 from which OSL sample XBMY-OSL-1 was collected. (d) Schematic of the excavated
750 sedimentary profile, with OSL sample positions and ages.

751 Fig. 3: Typical artefacts from the Xibaimaying site (Xie and Yu, 1989; Xie et al.,
752 2006): (a)–(e) scrapers, (f) and (g) points, (h) flake, (i) and (j) hammered core, (k)
753 and (l) percussion core, (m) bone tool.

754 Fig. 4: (a) Typical OSL decay curve and (b) dose response curve for a single grain of
755 quartz from sample XBMY-OSL-1. The dose response curves are fitted using a
756 single saturating exponential function of the form $I = I_0(1 - e^{-D/D_0}) + c$, where I is the
757 sensitivity-corrected OSL intensity, D is the regenerative dose, D_0 is the
758 characteristic saturation dose, and I_0 and c define the saturation value of the
759 exponential curve. The D_e is obtained by projecting the sensitivity-corrected natural
760 OSL signal (the upper point on the y-axis) on to the fitted curve and interpolating the
761 dose (dashed line).

762 Fig. 5: Results of the preheat temperature test on sample XBMY-OSL-5, conducted
763 using the single-aliquot regenerative-dose procedure in Table S1a. The D_e values
764 and corresponding recycling and recuperation ratios are plotted as a function of
765 preheat temperature in (a), (b) and (c), respectively. Each data point represents the
766 weighted mean for 13–20 aliquots and the vertical bars indicate the corresponding
767 1σ errors.

768 Fig. 6: (a) Distribution of measured (recovered) doses for all accepted grains in the
769 dose recovery test on sample XBMY-OSL-1, expressed as the ratio of recovered
770 dose to given dose (140 Gy). Open circles and closed triangles denote grains with
771 D_0 values of less than and more than 120 Gy (the optimum- D_0 threshold; see Table
772 S3), respectively. The grey band is centred on the weighted mean ratio (0.97 ± 0.04)
773 for the grains above the optimum- D_0 threshold of 120 Gy, calculated using the CAM,
774 which was also used to estimate the over-dispersion (OD) among the individual
775 recovered doses. (b) Mean dose recovery ratios (recovered dose/given dose) (red
776 squares) and the corresponding number of accepted grains (grey triangles) for
777 sample XBMY-OSL-1 plotted as a function of the D_0 threshold value. Ratios are
778 statistically consistent (at 2σ) with unity for all D_0 thresholds higher than 90 Gy.

779 Fig. 7: (a)–(d) D_e distributions for the accepted grains of samples XBMY-OSL-1, -2, -
780 3 and -5, respectively. Open circles and closed triangles denote D_e values for grains
781 with D_0 values below and above the optimum- D_0 thresholds, respectively. The grey
782 bands are centred on the weighted mean D_e values for the grains at and above the
783 optimum- D_0 thresholds.

784 Fig. 8: Weighted mean (CAM) D_e estimates (red squares) and the corresponding
785 number of accepted grains (grey triangles) plotted as a function of the D_0 threshold

786 value. The dashed lines indicate the CAM D_e values at the optimum- D_0 threshold for
787 each sample (150, 150, 120 and 30 Gy for samples XBMV-OSL-1, -2, -3 and -5,
788 respectively).

789 Fig. 9: Comparison of approximate ages reported previously for small-tool and
790 microlithic sites in the Nihewan Basin and the OSL ages obtained in this study for the
791 Xibaimaying site. The vertical grey band indicates the prevailing view that the small-
792 tool and microblade industries coexisted during the Upper Palaeolithic in the
793 Nihewan Basin, based on U-series dating of bovid teeth at Xiabimaying. The OSL
794 ages for Xibaimaying reported here imply a developmental trend from small-tool
795 technology (mid-MIS 3) to 'transitional' small/microlithic (Zhiyu, late MIS 3) to typical
796 microlithic technology (Youfang, early MIS 2) in the Nihewan Basin, denoted by the
797 dashed arrows. The oxygen isotope ($\delta^{18}\text{O}$) curve and Marine Isotope Stage (MIS)
798 boundaries follow Lisiecki and Raymo (2005). The age range of the Yujiagou site is
799 based on thermoluminescence (TL) dating of fine-grained quartz (Xia et al., 2001).

Table 1. Dose rates, D_e values and OSL ages for quartz grains from the Xibaimaying site.

Sample	Depth , m	Grain size, μm	Water, % ^a	U, ppm	Th, ppm	K, %	Environmental dose rate, Gy/ka ^b				D_e , Gy ^c	Age, ka
							Gamma	Beta	Cosmic	Total		
XBMY-OSL-1	2.8	125–150	15 ± 5	3.44 ± 0.15	10.99 ± 1.23	1.98	1.20 ± 0.08	1.82 ± 0.12	0.15 ± 0.03	3.21 ± 0.16	147.2 ± 7.5 (n = 89)	46 ± 3
XBMY-OSL-2	2.5	125–150	10 ± 3	4.15 ± 0.16	10.55 ± 1.22	2.02	1.33 ± 0.07	2.04 ± 0.08	0.17 ± 0.04	3.56 ± 0.12	112.4 ± 6.5 (n = 74)	32 ± 2
XBMY-OSL-3	2.0	125–150	10 ± 3	4.21 ± 0.17	9.74 ± 1.31	1.85	1.26 ± 0.07	1.96 ± 0.08	0.18 ± 0.04	3.42 ± 0.12	82.7 ± 7.5 (n = 32)	24 ± 2
XBMY-OSL-5	0.5	125–150	10 ± 3	3.67 ± 0.14	8.03 ± 1.04	1.61	1.08 ± 0.06	1.65 ± 0.07	0.20 ± 0.05	2.96 ± 0.10	39.3 ± 2.5 (n = 76)	13 ± 1

^a Time-averaged water contents for fluvial sample XBMY-OSL-1 and colluvial/aeolian samples XBMY-OSL-2, 3 and 5.

^b Dose rates corrected for water attenuation. The total dose rate also includes an internal dose rate of 0.03 ± 0.01 Gy/ka.

^c A systematic error of 2% has been added in quadrature to the D_e measurement error to allow for possible bias in the calibration of the laboratory beta source. The values in parentheses (n) indicate the number of the final accepted grains with D_0 values at and above the optimum- D_0 threshold.

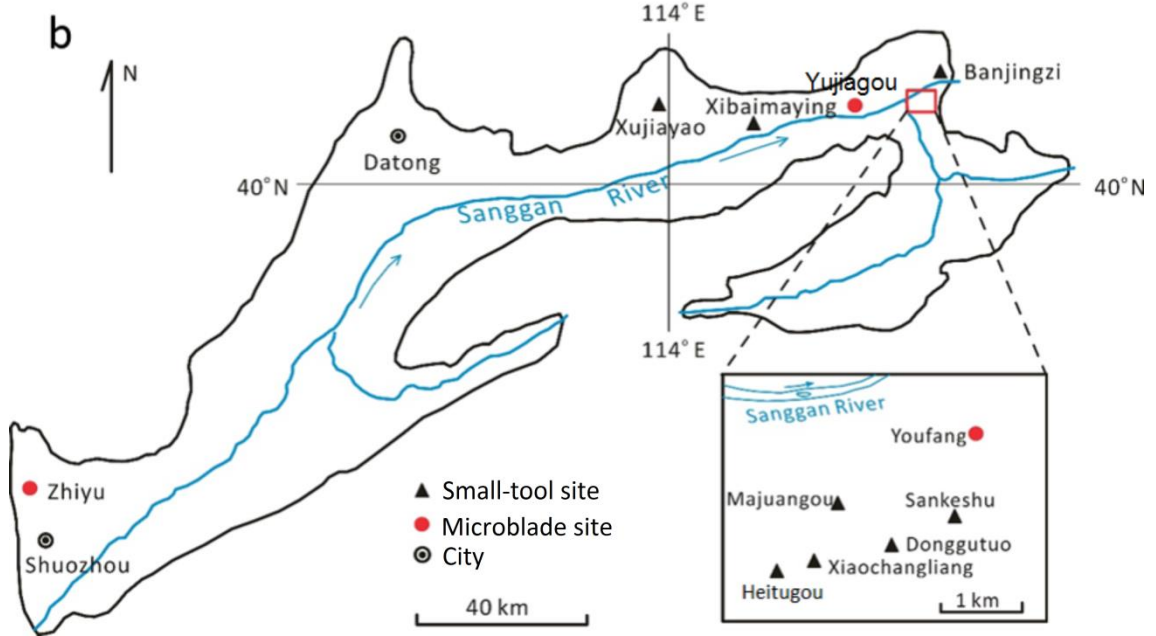
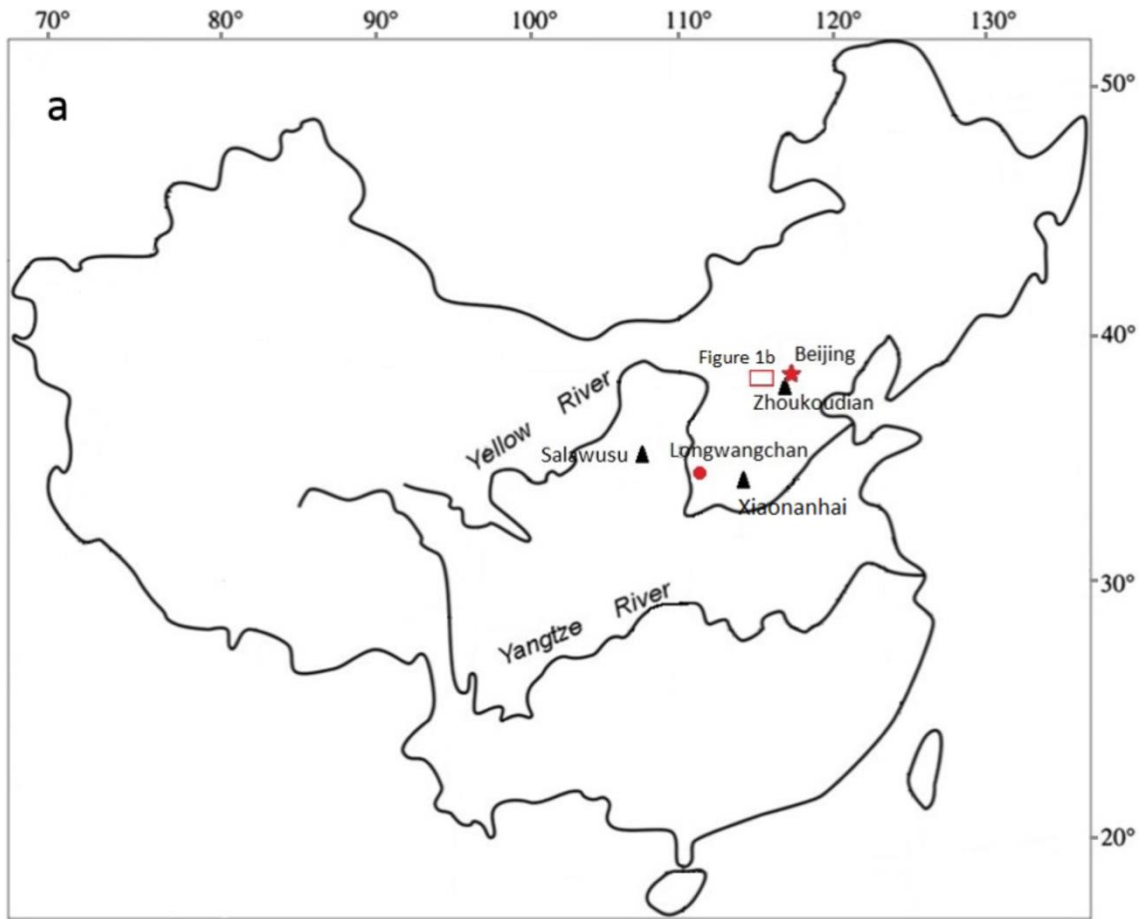


Fig. 1

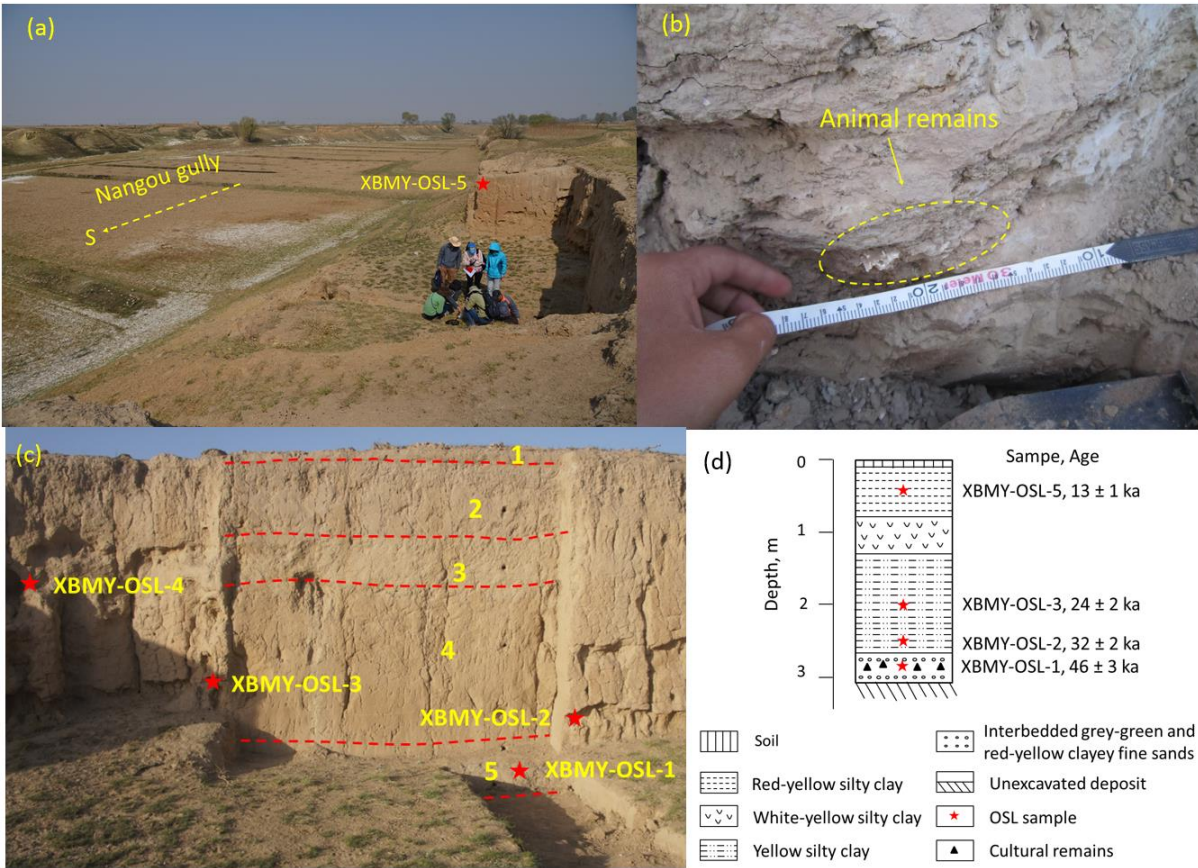


Fig. 2

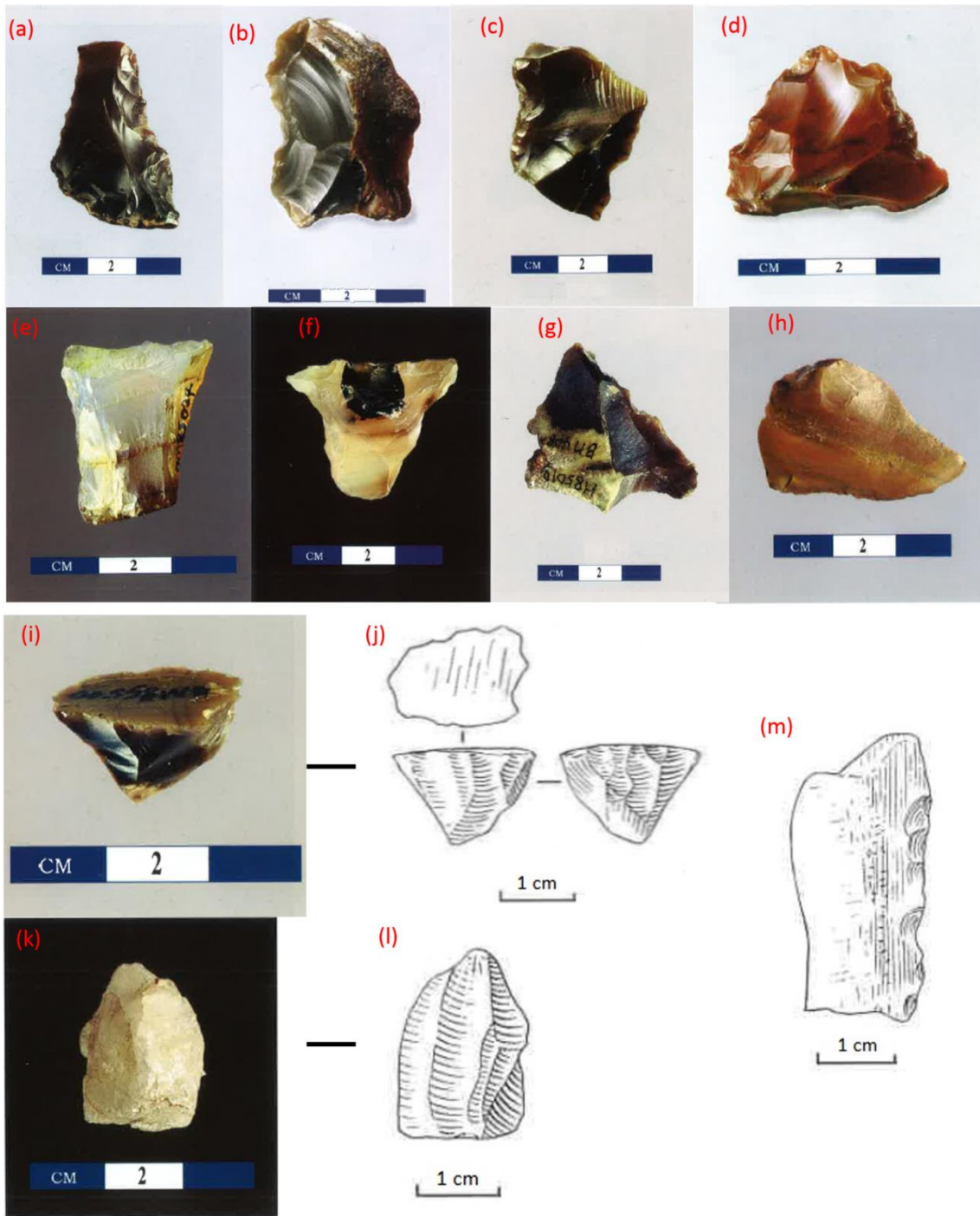


Fig. 3

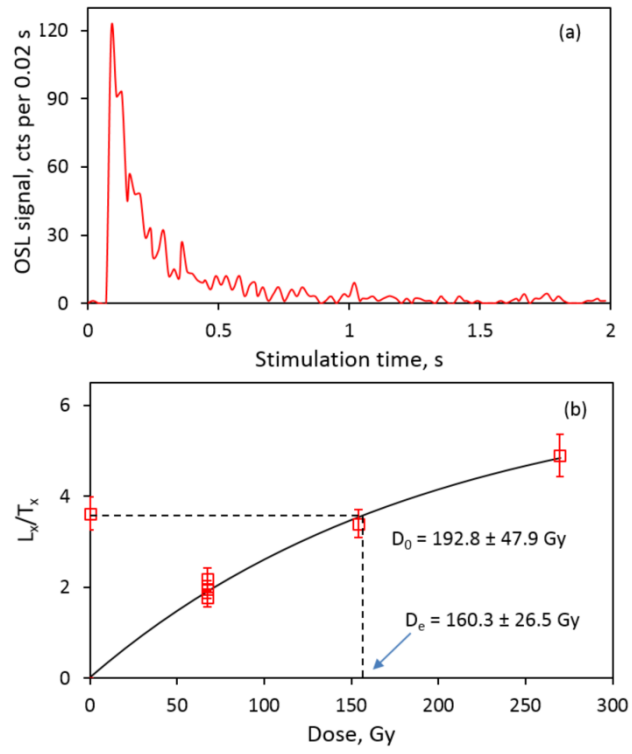


Fig. 4

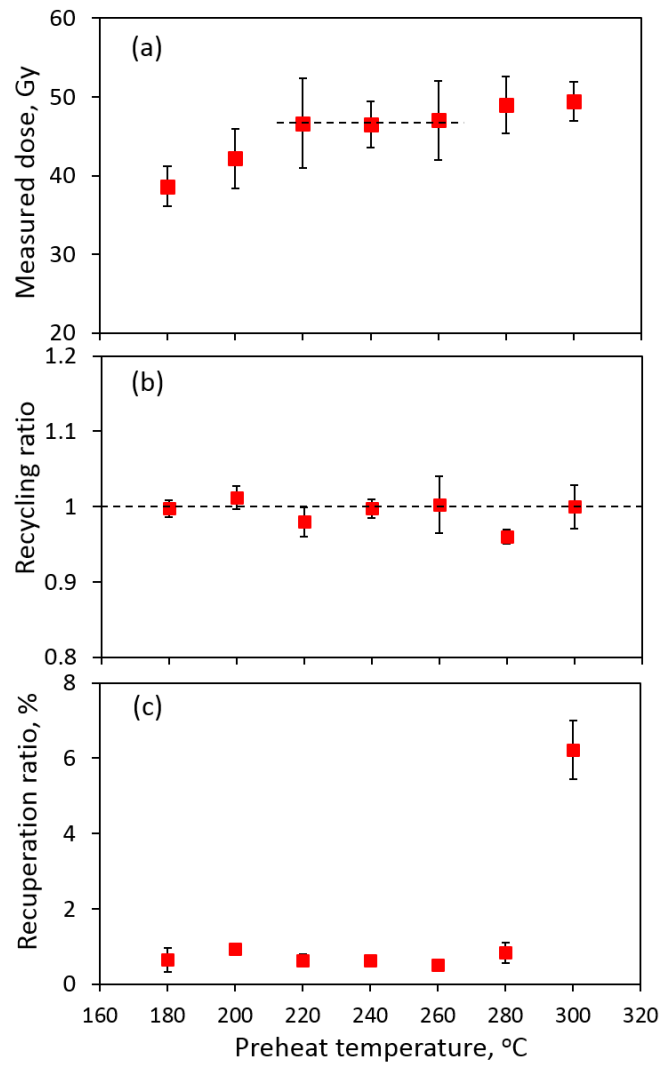


Fig. 5

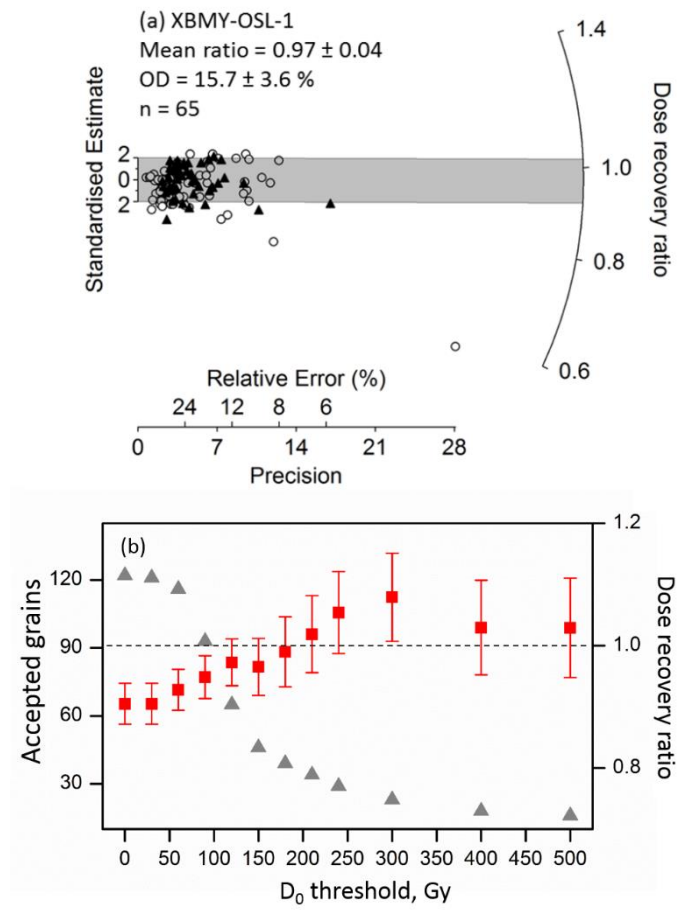


Fig. 6

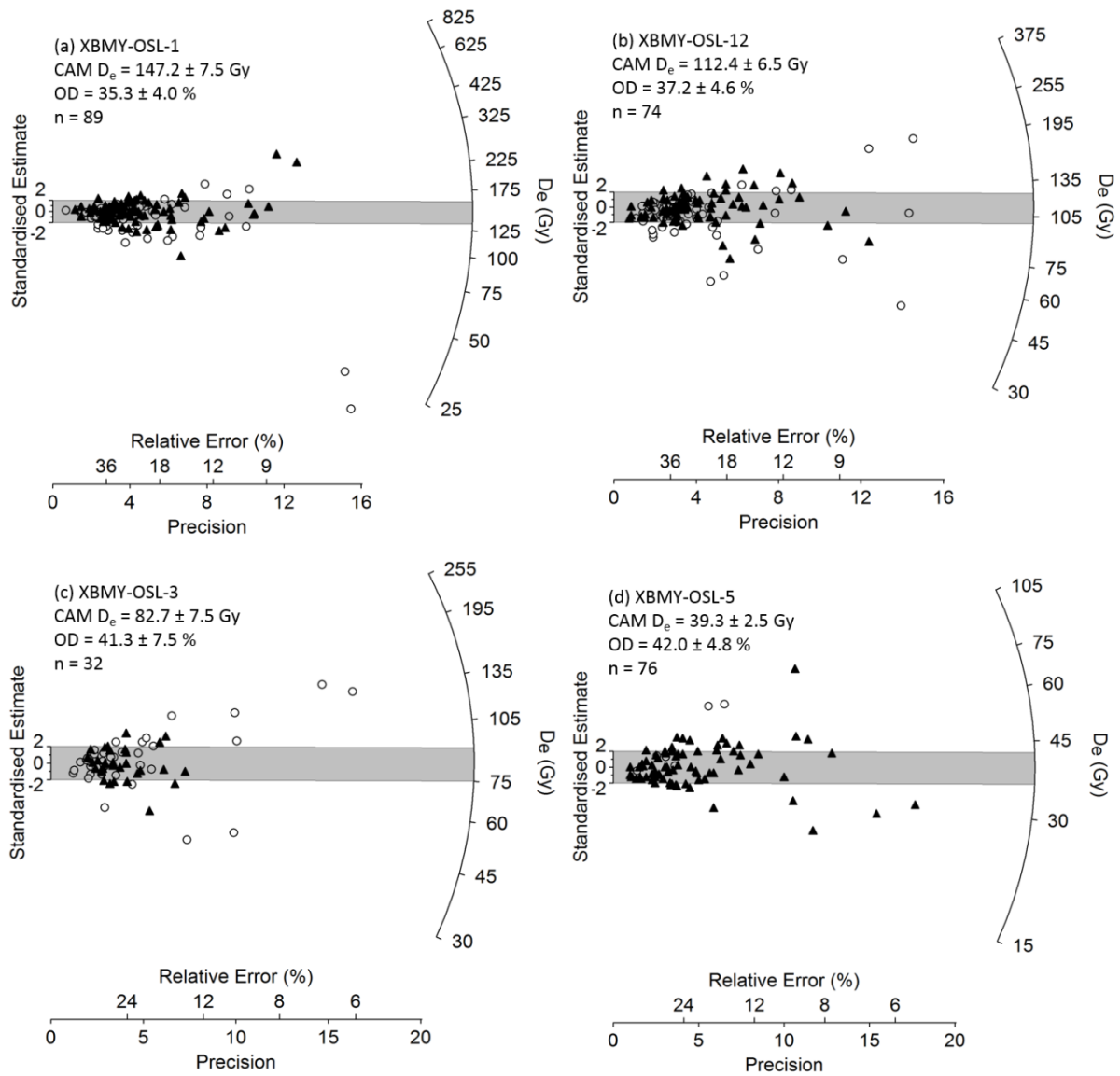


Fig. 7

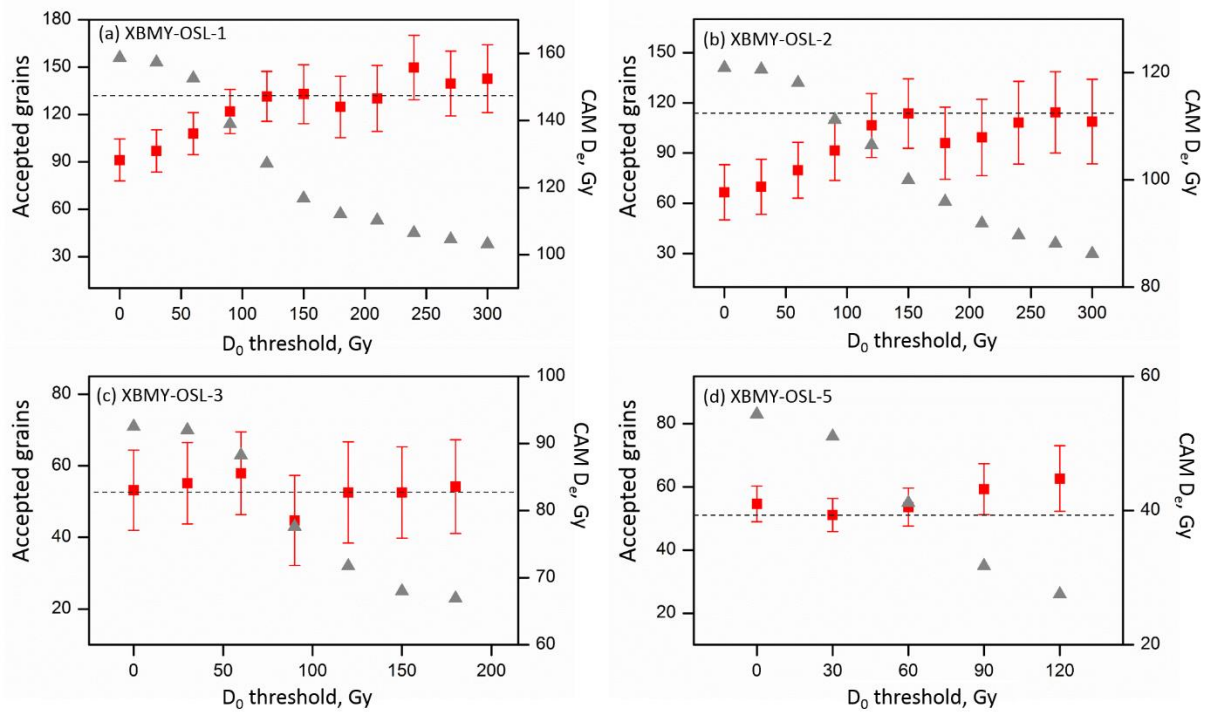


Fig. 8

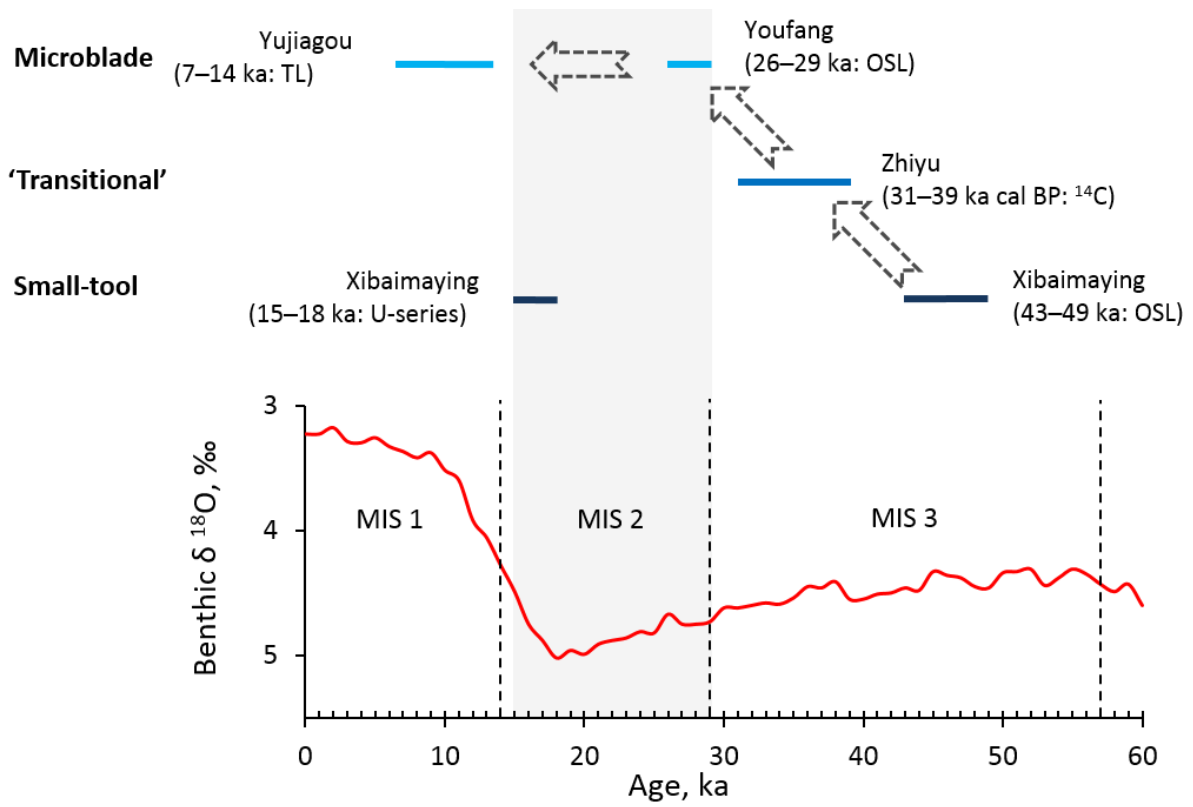


Fig. 9

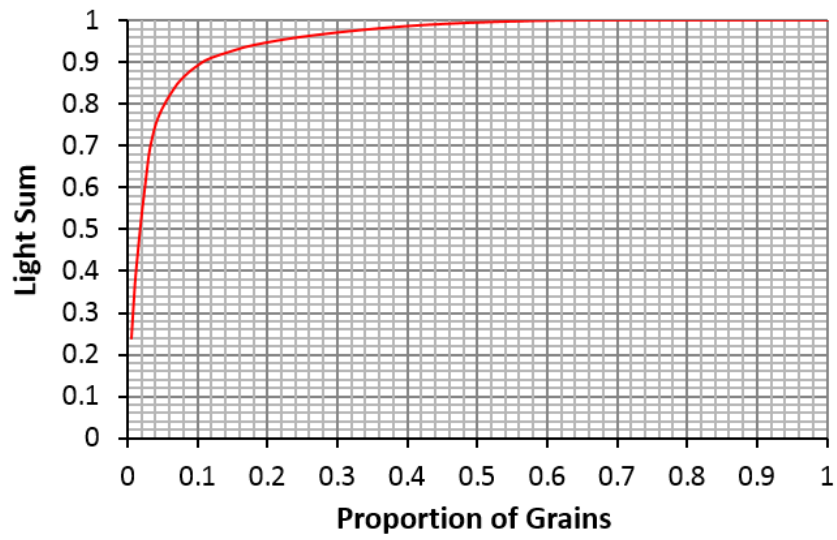


Figure S1 The single-grain 'brightness' distribution for 200 individual grains of sample XBMV-OSL-1. The cumulative light sum of the T_n signals (shown on the y-axis) is plotted as a function of the corresponding proportion of grains (shown on the x-axis).

Table S1 The single-aliquot regenerative-dose (SAR) procedures used in this study (based on Galbraith et al., 1999; Murray and Wintle, 2000, 2003).

(a) Single-aliquot procedure: preheat temperature test ^a		
Step	Treatment	Signal
1 ^b	Give regenerative dose, D_i	
2	Heat at 180–300 °C for 10 s	
3	Measure OSL at 125 °C for 40 s	L_n, L_x
4	Give test dose, D_t	
5	Heat at 20–40 °C lower than step 2 for 10 s	
6	Measure OSL at 125 °C for 40 s	T_n, T_x
7 ^c	Bleach at 20 °C higher than step 2 for 40 s	
8	Return to step 1	
(b) Single-grain procedure: dose recovery test and D_e estimation ^d		
Step	Treatment	Signal
1 ^b	Give regenerative dose, D_i	
2	Heat at 240 °C for 10 s	
3	Measure OSL at 125 °C for 1–2 s	L_n, L_x
4	Give test dose, D_t	
5	Heat at 200 °C for 10 s	
6	Measure OSL at 125 °C for 1–2 s	T_n, T_x
7 ^c	Bleach at 260 °C for 40 s	
8	Return to step 1	

^a The single-aliquot procedure was used to conduct a preheat temperature test on sample XBM5-OSL-5. The test dose preheat (step 5) was set 40 °C lower than the preheat applied to the natural and regenerative doses in step 2, except for the 180 °C preheat in step 2 which was accompanied by a test dose preheat of 160 °C in step 5.

^b For the natural dose, $i = 0$ and $D_i = 0$ Gy. The OSL signals induced by stimulation of the natural dose and its corresponding test dose are denoted L_n and T_n respectively, and the OSL signals induced by stimulation of the regenerative doses and their corresponding test doses are denoted L_x and T_x , respectively. The entire sequence is repeated for several regenerative doses, including a zero dose and a duplicate dose, to monitor the extent of recuperation and to determine the recycling ratio, respectively.

^c The 'hot optical bleach' in step 7 consists of OSL stimulation using blue light-emitting diodes with the sample held at a temperature 20 °C higher than the corresponding preheat in step 2.

^d A further (triplicate) regenerative dose cycle was included at the end of the single-grain SAR sequence to check for feldspar contamination of individual quartz grains on the basis of their OSL IR depletion ratios (Duller, 2003). The regenerative dose was stimulated using infrared light-emitting diodes for 40 s at 50 °C prior to stimulation of the OSL signal using a green laser.

Table S2 Number of individual quartz grains measured, rejected and accepted for D_e determination, and the reasons for their rejection.

Sample	No. of grains measured	Weak T_n signal or test dose error >25% ^a	Recuperation ratio >10% ^c	Poor recycling ratio or OSL IR depletion ratio ^d	Poor DRC fit to L_x/T_x ^e	L_n/T_n consistent with or above saturation ^f	Sum of rejected grains	No. of grains accepted for D_e estimation
dose recovery test ^g	2000	1715	11	101	2	49	1878	122
XBMY-OSL-1	3400	3066	9	118	5	46	3244	156
XBMY-OSL-2	2800	2492	63	53	10	41	2659	141
XBMY-OSL-3	1400	1267	23	28	2	9	1329	71
XBMY-OSL-5	1900	1738	17	60	0	2	1815	83

^a Initial 0.12 s of the T_n signal is less than 3 times the corresponding background (determined from the last 0.12 s of stimulation).

^b Relative error on the T_n signal exceeds 25%.

^c Extent of recuperation (ratio of zero dose L_x/T_x signal to the L_n/T_n signal, expressed as a percentage) exceeds 10%.

^d Recycling ratio or the OSL IR depletion ratio differs from unity by more than 2σ .

^e DRC is an obviously poor fit to the L_x/T_x data points.

^f L_n/T_n signal consistent with or exceeding the saturation level of the corresponding DRC (i.e., does not intersect the DRC), and, hence, no finite estimate of D_e can be obtained.

^g Conducted on sample XBMY-OSL-1.

Table S3 Central Age Model (CAM) D_e values, over-dispersion values, and number of accepted and saturated grains at various characteristic saturation dose (D_0) thresholds. The optimum- D_0 threshold values are highlighted in bold.

Sample	D_0 threshold (Gy)	No. of grains with L_n/T_n values consistent with or above saturation	No. of grains used for D_e estimation	CAM D_e (Gy)	Over-dispersion (%)
XBMY-OSL-1 dose recovery test	0	49	122	126.7 ± 4.7	23.5 ± 2.9
	30	35	121	126.7 ± 4.7	23.5 ± 2.9
	60	20	116	129.9 ± 4.7	21.4 ± 2.9
	90	8	93	132.8 ± 4.9	18.5 ± 3.1
	120	0	65	136.2 ± 5.3	15.7 ± 3.6
	150		46	138.6 ± 8.0	19.3 ± 4.4
	180		39	142.6 ± 8.8	23.1 ± 5.3
	210		34	145.1 ± 8.4	22.3 ± 6.0
	240		29	147.6 ± 9.3	18.9 ± 6.9
	300		23	151.1 ± 10.1	16.1 ± 7.9
	400		18	144.1 ± 10.8	17.8 ± 8.3
500		16	144.1 ± 11.4	18.6 ± 8.4	
XBMY-OSL-1	0	46	156	128.2 ± 6.2	47.4 ± 3.6
	30	40	153	130.9 ± 6.3	45.9 ± 3.5
	60	19	143	136.1 ± 6.2	40.9 ± 3.4
	90	4	114	142.6 ± 6.6	36.1 ± 3.5
	120	0	89	147.2 ± 7.5	35.3 ± 3.9
	150		67	147.8 ± 8.8	38.2 ± 4.7
	180		57	144.0 ± 9.1	37.6 ± 5.1
	210		53	146.6 ± 9.8	38.4 ± 5.4
	240		45	155.8 ± 9.6	29.5 ± 5.3
	270		41	151.0 ± 9.7	29.2 ± 5.5
	300		38	152.4 ± 10.1	29.3 ± 5.7
	0	41	141	97.7 ± 5.2	48.4 ± 4.0

XBMY-OSL-2	30	37	140	98.7 ± 5.1	47.4 ± 3.9
	60	24	132	101.8 ± 5.2	44.3 ± 3.9
	90	9	110	105.5 ± 5.6	41.7 ± 4.1
	120	2	95	110.2 ± 6.0	39.4 ± 4.2
	150	0	74	112.4 ± 6.5	37.2 ± 4.6
	180		61	106.8 ± 6.7	37.3 ± 5.0
	210		48	107.9 ± 7.1	33.9 ± 5.5
	240		41	110.7 ± 7.7	32.9 ± 5.8
	270		36	112.6 ± 7.6	27.5 ± 6.0
	300		30	110.9 ± 7.9	25.4 ± 6.7
XBMY-OSL-3	0	9	71	83.0 ± 5.6	49.6 ± 5.6
	30	6	70	84.1 ± 5.6	49.2 ± 5.6
	60	4	63	85.5 ± 5.7	46.5 ± 5.7
	90	1	43	78.5 ± 6.9	45.6 ± 6.9
	120	0	32	82.7 ± 7.5	41.3 ± 7.5
	150		25	82.7 ± 7.3	29.8 ± 7.3
	180		23	83.6 ± 7.5	28.5 ± 7.5
210		17	79.5 ± 8.6	27.4 ± 8.6	
XBMY-OSL-5	0	2	83	41.0 ± 2.7	46.4 ± 4.9
	30	0	76	39.3 ± 2.5	42.0 ± 4.8
	60		55	40.5 ± 2.8	39.3 ± 5.5
	90		35	43.2 ± 3.8	40.4 ± 7.2
120		26	44.8 ± 4.9	45.3 ± 8.9	